



HAL
open science

On wave breaking for Boussinesq-type models

Maria Kazolea, Mario Ricchiuto

► **To cite this version:**

Maria Kazolea, Mario Ricchiuto. On wave breaking for Boussinesq-type models. [Research Report] RR-9092, INRIA. 2017, pp.37. hal-01581954

HAL Id: hal-01581954

<https://inria.hal.science/hal-01581954>

Submitted on 5 Sep 2017

HAL is a multi-disciplinary open access archive for the deposit and dissemination of scientific research documents, whether they are published or not. The documents may come from teaching and research institutions in France or abroad, or from public or private research centers.

L'archive ouverte pluridisciplinaire **HAL**, est destinée au dépôt et à la diffusion de documents scientifiques de niveau recherche, publiés ou non, émanant des établissements d'enseignement et de recherche français ou étrangers, des laboratoires publics ou privés.



On wave breaking for Boussinesq-type models

Maria Kazolea, Mario Ricchiuto

**RESEARCH
REPORT**

N° 9092

September 2017

Project-Teams CARDAMOM

ISRN INRIA/RR--9092--FR+ENG

ISSN 0249-6399



On wave breaking for Boussinesq-type models

Maria Kazolea*, Mario Ricchiuto †

Project-Teams CARDAMOM

Research Report n° 9092 — September 2017 — 37 pages

Abstract: We consider the issue of wave breaking closure for Boussinesq type models, and attempt at providing some more understanding of the sensitivity of some closure approaches to the numerical set-up. In particular, we are interested in the potential for mesh refinement, and in quantifying the dissipation mechanism active. Two closure strategies are considered. The first is an eddy viscosity approach following some early work by O. Nwogu in the 90's, and some more recent developments by Zhang and co-workers. In this model, a breaking viscosity is computed starting from a turbulent kinetic energy. The latter is obtained from an ad-hoc partial differential equation, which is solved in parallel with the propagation model. The second approach considered consists in suppressing the dispersive terms in breaking regions. The dissipation of total energy obtained in a shallow water shock is used to model the energy dissipation due to breaking. Due to its simplicity and effectiveness, the second approach has gained substantial attention in the coastal engineering community. Here we propose a systematic comparison of the two approaches, to understand more of their sensitivity w.r.t. the type of propagation model used (weakly or fully non-linear), to the type of breaking wave being simulated, as well as to understand the mesh dependence of the pointwise results obtained, and in particular the potential for achieving mesh converged simulations. Finally, we provide a quantitative analysis of the dissipation introduced by the two closures for a moving breaking bore.

Key-words: wave breaking, eddy viscosity, hybrid, comparison, Green-Naghdi equations, Nwogu equations

* maria.kazolea@inria.fr

† mario.ricchiuto@inria.fr

**RESEARCH CENTRE
BORDEAUX – SUD-OUEST**

200 avenue de la Vieille Tour
33405 Talence Cedex

On wave breaking for Boussinesq-type models

Résumé : Ce travail considère la question de la simulation des vagues déferlantes en utilisant les modèles de type Boussinesq. On tente de mieux comprendre la sensibilité de certaines approches de fermeture pour le déferlement à l'approximation numérique. En particulier, nous sommes intéressés par le potentiel pour le raffinement du maillage, et la quantification et détermination du mécanisme de dissipation responsable pour le déferlement. Deux stratégies de fermeture sont implémentées. La première est une approche de type "eddy viscosity". Nous reformulons un modèle d'évolutions pour l'énergie cinétique turbulente initialement proposé par Nwogu et des développements plus récents de Zhang et de ses collègues.

Dans ce modèle, une viscosité artificielle est calculée par une équation d'énergie cinétique turbulente. La deuxième approche consiste à supprimer les termes de dispersion dans les régions déferlantes. La dissipation de l'énergie totale obtenue dans un choc modélise la dissipation d'énergie provoquée par le déferlement. La deuxième approche a une attention considérable dans la communauté d'ingénierie côtière.

Nous proposons ici une comparaison systématique des deux approches POUR tenter de mieux comprendre leur sensibilité au type de modèle de propagation utilisé, et au type de déferlement (spilling, plunging, etc). Nous voulons comprendre la dépendance au maillage des résultats ponctuels obtenus.

Mots-clés : wave breaking, eddy viscosity, hybrid, comparaison, Green-Naghdi equations, Nwogu equations

Contents

1	Introduction	3
2	Wave propagation models	5
2.1	The weakly nonlinear-weakly dispersive model of Nwogu	5
2.2	Fully nonlinear-weakly dispersive Green-Naghdi equations	6
3	Numerical discretization of the Boussinesq models	7
4	Wave breaking closure	8
4.1	Hybrid wave breaking model	9
4.2	Wave breaking closure via a PDE based TKE model	10
5	Boundary condition and the internal source function	12
6	Numerical results	13
6.1	Wave breaking over a bar	13
6.2	Solitary waves breaking on a slope	17
6.3	Wave height and setup prediction	18
6.4	Breaking of a dichromatic wave train	22
6.5	Propagation, breaking, and overtopping of a 2D reef	24
6.6	Breaking bore propagation and energy dissipation	27
7	Conclusions	29

1 Introduction

The last decades have seen the development of several numerical models allowing the simulation of wave propagation from intermediate depths to shallow water by means of some set of depth averaged Boussinesq-type (BT) equations. These models allow to accurately simulate the dispersive propagation and shoaling of free surface waves, within some asymptotic error w.r.t. nonlinearity and dispersion parameters depending on wave amplitude, wavelength and depth. The reader may refer to the reviews [13, 45] for a broad discussion, and the book [47] for the fundamental aspects concerning the derivation of the models. Being obtained under the hypotheses of ideal and irrotational flow, these models cannot account for the production and for the evolution of vorticity taking place in breaking regions. To cope with this limitation, some closure model needs to be introduced.

At large scales, the main consequence of wave breaking is a strong energy dissipation. So the first attempt to simulate wave breaking was proposed by Zelt [94] introducing a dissipation term in the momentum equation. This term controls the dissipation of energy produced by the wave breaking and it is governed by the value of an eddy viscosity coefficient which must be calibrated with experimental data. Of course, different calibration is needed for different sets of equations. Moreover, to initiate and/or terminate the breaking process some breaking detection criterion needs to be used to activate this eddy viscosity term. The same approach has been followed by many researchers, see for example [41, 68, 87, 36, 51, 52]. One of the criticisms to this approach is that, while simple, no direct physical meaning can be attributed to the scaling coefficients involved in the definition of the viscosity [18]. A more relevant physical definition of the effects of breaking on the large scale flow has been attempted using the so-called roller models (see e.g. [72, 71, 55]). While based on a better physical background,

these models still rely on an algebraic ad-hoc definition of a momentum dissipation, and require an appropriate calibration. A more advanced version of these roller models has been proposed in [12], and more recently extended in [83]. These models attempt at accounting for depth variations of some of the physical quantities (eddy viscosity, horizontal velocity), thus going beyond the irrotational hypothesis when computing the vorticity and/or dissipation generated in breaking regions. While promising in principle, these models are quite complex to implement, require an additional vertical discretization, and have so far been applied only to simple configurations. We also mention the related work presented in [15, 49] in which BT models with vorticity effects are discussed. In our view, beside the necessity of calibrating the eddy viscosity, drawbacks of the models discussed above are related both to the unclear relation between numerical and physical dissipation, as well as to their inability to describe properly some special cases as, e.g. stationary hydraulic jumps. To the authors' knowledge there is very little evidence in literature that this type of breaker can be easily modelled with the eddy viscosity approach. Results embedding this type of features, such as e.g. the 2D reef computations presented in [68], are always computed on one mesh. This makes unclear whether the major effect observed is that of the model or that of the limiter/numerical dissipation.

A more sound and efficient method would be to define the breaking dissipation through some turbulence model involving partial differential equations for the main physical quantities: turbulent kinetic energy, energy dissipation, eddy viscosity, and so on. To our knowledge so far only [29, 23, 95, 64, 27] have adopted this path, with only [29, 23, 95] actually focusing on complex cases.

As an alternative to the use of eddy viscosity, the last ten years have seen the development of a new hybrid approach. It is a simple method in which in appropriately detected breaking regions the dispersive terms are suppressed and the non linear shallow water (NSW) equations are solved. The dissipation of total energy obtained in a shallow water shock is used to model the energy dissipation due to breaking. Due to its relative simplicity and effectiveness, this approach has gained substantial attention in the coastal engineering community, see for example [79, 39, 24, 48, 69, 70]. The idea was first introduced in [79] in order to exploit the Finite Volume (FV) technique as to simulate discontinuous phenomena such as wave breaking and run-up. In the same work, an indicator criterion for breaking has been extracted based on the similarity between spilling breakers and bores. This criterion has been proven inadequate in some cases [39, 44] since its use leads to less energy dissipation than needed. Several more sophisticated criteria have been developed based on physical or numerical arguments [11, 39, 6, 21]. As pointed out in [24], this approach has a major limitation in the stability of the coupling which introduces spurious oscillations at the interface between the breaking and no-breaking region. For all the current implementations of this closure, the ability to achieve grid convergence of the point values of the solution remains unclear. There exist in literature no grid convergence analyses, perhaps with the only exception of the single computation shown in [70] in which the authors observe convergence in time averaged quantities, but report the appearance of increasing oscillations in the pointwise values of the solution without further notice. This point needs to be clarified if one wishes to use mesh adaptation techniques to better resolve breaking fronts.

The aim of this work is to study and compare a turbulence model closure for wave breaking with the hybrid approach. We want to investigate the sensitivity of the two approaches w.r.t. the type of propagation model used (weakly or fully non-linear), with the type of breaking wave being simulated, as well as the mesh dependence of the models and of the pointwise results, and in particular the potential for achieving mesh converged simulations. We also want to compare the magnitude and the impact of numerical versus breaking model dissipation. As a basis for the study, we will use the numerical models developed in [37, 38] and [24, 25], providing both a weakly-nonlinear and a fully nonlinear description weakly-dispersive wave propagation. The paper will in particular focus on one-dimensional tests. Concerning the choice of the turbulence model, we have opted for the one equation model proposed in

[29, 23, 95] coupled with a wave breaking detector proposed in [39, 24], and also used for the hybrid method. Our results show that, with the implementation proposed in this paper, and as long as the mesh is coarse enough, the two closures provide very similar results, and present a very similar dependence of the wave breaking (and model) parameters. However, as soon as mesh refinement is attempted, only a careful implementation of the turbulence model allows to obtain mesh converged results, while the hybrid approach gives very oscillatory solutions, or blows up. We also provide a quantitative analysis of the dissipation introduced by the scheme, and by the model when relevant, for a moving breaking bore. The results allow to confirm that, independently on the mesh size, when using the eddy viscosity approach the model dissipation is way more important than that of the numerical scheme, which is otherwise dominant in the hybrid approach.

The paper is organised as follows. Section two presents the two Boussinesq approximations used in this work. Section 3 discusses the numerical approximation of the models, as well as of the wave breaking closure. The comparison of the two approaches on a wide selection of benchmarks is discussed in section 4. The paper is ended by a summary and a sketch of the future and ongoing developments of this work.

2 Wave propagation models

2.1 The weakly nonlinear-weakly dispersive model of Nwogu

With the notation sketched in figure 1, we consider the Boussinesq equations proposed by Nwogu [60] based on a weakly-dispersive and weakly-nonlinear asymptotic approximation in terms of the velocity u^a at an arbitrary distance from a still water level z^a . Denoting partial derivatives with respect to space and time with the subscripts x and t , Nwogu's equations can be cast in a balance law form as follows

$$\mathbf{U}_t + \mathbf{F}(\mathbf{U}^*)_x = \mathbf{S}_b - \mathbf{S}_d + \mathbf{S}_f + \mathbf{R}_{wb}, \quad (1)$$

where \mathbf{U} is the vector of the new variables, \mathbf{U}^* is the vector of the conserved variables, and \mathbf{F} is the flux vector

$$\mathbf{U} = \begin{bmatrix} H \\ P^* \end{bmatrix}, \quad \mathbf{F}(\mathbf{U}) = \begin{bmatrix} Hu^a \\ H(u^a)^2 + \frac{1}{2}gH^2 \end{bmatrix}.$$

The P^* variable is a pseudo-mass flux accounting for the vertical (weakly-dispersive and weakly-nonlinear) expansion of the velocity profile:

$$P^* = Hu^a + Hz^a \left(\frac{z^a}{2} u_{xx}^a + (du^a)_{xx} \right) \quad (2)$$

In the above equations d denotes the still water depth, $H(x, t) = d(x) + \eta(x, t)$ the total water depth, $\eta(x, t)$ the free surface elevation, b the bathymetry height, g is the gravitational acceleration. As done usually, the value of z^a is chosen to optimize the linear dispersion properties of the model, namely $z^a = -0.531d$.

The three source terms on the right hand side of (1) can be expressed as $\mathbf{S}_b = [0 \quad -gHb_x]^T$, accounting for the effects of the shape of the topography, $\mathbf{S}_f = [0 \quad -gHS_f u^a]$ with $S_f = \frac{n_m^2 ||u||}{H^{4/3}}$, accounting for the friction on the bottom, and $\mathbf{S}_d = [\psi_C \quad u^a \psi_C - \psi_M]$ introduces additional dispersive terms which do not contain time derivatives, and in particular

$$\psi_M = -((Hu^a)_x + \psi_C)z^a \left(\frac{z^a}{2} u_{xx}^a + (du^a)_{xx} \right), \quad \psi_C = \left[\left(\frac{(z^a)^2}{2} - \frac{d^2}{6} \right) du_{xx}^a + \left(z^a + \frac{d}{2} \right) d(du^a)_{xx} \right]_x. \quad (3)$$

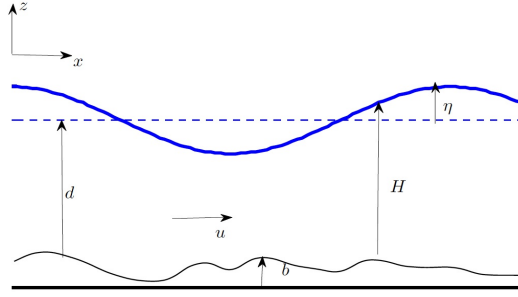


Figure 1: Sketch of the domain.

The last term on the right hand side is the turbulent wave breaking term, which is only present when this approach is activated. Following [29, 23, 95] this term has the form

$$\mathbf{R}_{\mathbf{wb}} = \begin{bmatrix} 0 \\ r_{wb} \end{bmatrix}_x, \quad r_{wb} = \nu_t H u_x^a$$

with the eddy viscosity ν_t computed from the discretization of the turbulence model, discussed in §4.2.

2.2 Fully nonlinear-weakly dispersive Green-Naghdi equations

To account for fully nonlinear effects, we also consider the Green-Naghdi (GN) partial differential equations [28]. In particular, we cast the system in the form suggested in [24] (see also [3, 10, 47] and references therein) :

$$H_t + (Hu)_x = 0 \quad (4)$$

$$(Hu)_t + (Hu^2)_x + gH\eta_x = H\psi \quad (5)$$

$$H\psi + \alpha HT(\psi) = HT(w) - H\mathcal{Q} + gHS_f u + (r_{wb})_x \quad (6)$$

where now u denotes the depth averaged velocity, with $w = g\eta_x$, and \mathcal{T} a linear elliptic operator with the self-adjoint form [3]

$$\mathcal{T}(\cdot) = S_1^* (HS_1(\cdot)) + S_2^* (HS_2(\cdot)), \quad (7)$$

where in one space dimension

$$S_1 = \frac{H}{\sqrt{3}}(\cdot)_x - \frac{\sqrt{3}}{2}b_x(\cdot), \quad S_2 = \frac{1}{2}b_x(\cdot). \quad (8)$$

The right hand side last in (6) also introduces the nonlinear forcing \mathcal{Q} defined as

$$\mathcal{Q} = 2HH_x(u_x)^2 + \frac{4H^2}{3}u_x u_{xxx} + Hb_x(u_x)^2 + Hb_{xx}uu_x + \left[b_{xx}H_x + \frac{1}{2}Hb_{xxx} + b_x b_{xx} \right] u^2 \quad (9)$$

Following [48] the value $\alpha = 1.159$ is chosen to optimise the linear dispersion relation of the system. In absence of friction and of turbulent dissipation, the above system can be solved in two independent steps: the first to invert the elliptic operator $I + \alpha\mathcal{T}$, the second to evolve physical quantities by solving the shallow water equations with the algebraic dispersive correction $H\psi$.

3 Numerical discretization of the Boussinesq models

The numerical treatment of both systems introduced above is done using an implicit treatment of the dissipative components (friction and/or turbulent dissipation). In particular, the kernel of both models is the hyperbolic component which rules the evolution of the water level and flux variables. Consider then non-overlapping temporal slabs $[t^n, t^{n+1}]$, with $\Delta t^{n+1} = t^{n+1} - t^n$. The hyperbolic evolution is performed with the two-stages Adams Bashforth-Adams Moulton predictor-corrector method which, for the ODE $U' = \mathcal{L}(U)$ reads:

1. Predictor stage (Adams-Basforth method)

$$\mathbf{U}^P = \mathbf{U}^n + \Delta t \mathcal{L}^P, \quad \mathcal{L}^P = \frac{23}{12} \mathcal{L}(\mathbf{U}^n) - \frac{16}{12} \mathcal{L}(\mathbf{U}^{n-1}) + \frac{5}{12} \mathcal{L}(\mathbf{U}^{n-2}) \quad (10)$$

2. Corrector stage (Adams-Moulton method)

$$\mathbf{U}^{n+1} = \mathbf{U}^n + \Delta t \mathcal{L}^C \quad \mathcal{L}^C = \frac{9}{24} \mathcal{L}(\mathbf{U}^P) + \frac{19}{24} \mathcal{L}(\mathbf{U}^n) - \frac{5}{24} \mathcal{L}(\mathbf{U}^{n-1}) + \frac{1}{24} \mathcal{L}(\mathbf{U}^{n-2}) \quad (11)$$

with the time step is computed by means of the standard condition $\Delta t^{n+1} = \text{CFL} \Delta x / \max_i (|u_i^n| + \sqrt{gh_i^n})$. Within both stages, the evolution operator \mathcal{L} accounts for all the effects except those of friction and turbulent dissipation (if present). In particular, the shallow water terms are approximated by means of a third order MUSCL finite volume approximation [85, 42], with Roe-type numerical fluxes [66]. It is useful for some of the analysis that will follow to report the form of these fluxes reading :

$$\begin{aligned} \mathcal{L}_i^{SW} &= -\frac{1}{\Delta x} (\mathbf{F}_{i+1/2} - \mathbf{F}_{i-1/2}) + \Delta \mathbf{S}_{\mathbf{b}_i}^{i+1/2} + \Delta \mathbf{S}_{\mathbf{b}_i}^{i-1/2} \\ \mathbf{F}_{i+1/2} &= \frac{1}{2} \left(\mathbf{F}(\mathbf{U}_{i+1/2}^R) + \mathbf{F}(\mathbf{U}_{i+1/2}^L) \right) - \frac{1}{2} |\mathbf{A}|_{i+1/2} \Delta_{i+1/2} \mathbf{U} \end{aligned} \quad (12)$$

where $\Delta(\cdot)_{i+1/2} = (\cdot)_{i+1/2}^R - (\cdot)_{i+1/2}^L$, and $|\mathbf{A}|_{i+1/2}$ is the usual absolute value of the shallow water flux Jacobian, computed via eigenvalue decomposition, and modified with with an entropy fix [32, 34]. The source term contributions $\Delta \mathbf{S}_{\mathbf{b}_i}^{i\pm 1/2}$ are well balanced, and involve both a centered and an upwind approximation of the gradient of the bathymetry. We omit details concerning this (quite classical) aspect, for which the interested reader can consult [8, 16, 37, 22, 5] and references therein.

Concerning the dispersive terms, the \mathbf{S}_d contribution in (1) is discretized using finite differences. While for the hyperbolic component the minimization of the dispersion error requires at least a third order approximation, this is not the case for the higher derivatives in the dispersive terms (see [86, 24] for more details on this issue). Here, following [37], the second and third order derivatives in (1) are treated by means of second order central differencing. Similarly, the dispersive correction ψ in the GN system (4)-(6) is evaluated by means of a second order P^1 continuous finite element approximation of the operator $H + \alpha H \mathcal{T}$ and of the nonlinear forcing term \mathcal{Q} . In absence of friction and turbulent dissipation, equation (6) can be simplified by dividing through by H , and the self adjoint character of \mathcal{T} (equations (7) and (8)) can be used to deduce a simple variational form reading

$$\int_{\Omega} (v\psi + S_1(v)HS_1(\psi) + S_2(v)HS_2(\psi)) = \int_{\Omega} (S_1(v)HS_1(w) + S_2(v)HS_2(w)) + Q(v)$$

The last expression immediately allows to recover the three diagonal system for the unknown ψ which is symmetric and positive semi-definite. The term Q on the right hand side is the variational form of the

forcing term (9) for which we refer to the full expressions given in [24, 25].

The effects of friction and turbulent dissipation (if present) are now embedded in an implicit manner, by appropriately correcting the velocity values. In particular, for Nwogu's equations, the stage iterations (10) and (11) are modified as follows:

$$\mathbf{U}^{new} - \Delta t \mathbf{S}_f^{new} - \Delta t \mathbf{R}_{wb}^{new} = \mathbf{U}^n + \Delta t \mathcal{L}$$

Accounting for the definitions of the source terms, and of the pseudo mass-flux P^* in (2), we obtain the following operator defining the new velocity values (the superscript a is dropped for simplicity)

$$\begin{aligned} H^{new} (u^{new} + z^a \left(\frac{z^a}{2} u_{xx}^{new} + (d u^{new})_{xx} \right)) + \Delta t g S_f(H^{new}, u^*) u^{new} - \Delta t (\nu_t^* H^{new} u_x^{new})_x \\ = H^n u^n + H^n z^a \left(\frac{z^a}{2} u_{xx}^n + (d u^n)_{xx} \right) + \Delta t \mathcal{L}_{Hu} \end{aligned} \quad (13)$$

where \mathcal{L}_{Hu} is the second component of \mathcal{L} , u^* and ν_t^* are the last available values of the velocity and turbulent viscosity, and H^{new} is independently computed from the first discretized equation. As before, the derivatives present in (13) are discretized using second order central finite differences, yielding a tri-diagonal system for the new value of the velocity at each stage.

The implementation has been slightly modified for the GN equations. In this case we have added after each of the iterations (10) and (11) a split (in time) implicit discretization of $\mathbf{U}_t = \mathbf{S}_f^{new} + \mathbf{R}_{wb}^{new}$. Denoting by u^* the last known value of the velocity (after (10) and/or (11)), we thus obtain the expression

$$H^{new} \frac{u^{new} - u^*}{\Delta t} + g H^{new} S_f(H^{new}, u^*) u^{new} = (\nu_t^* H^{new} u_x^{new})_x.$$

The derivatives in the above expression are then approximated by second order finite differences, leading to a tri-diagonal system again. As in this case the evaluation of the dispersive correction ψ already requires the inversion of a linear system, we have opted here for a simplified implementation involving a few explicit Jacobi relaxation iterations which read

$$\begin{aligned} J_i^m \left((u^{new})^{m+1} - (u^{new})^m \right)_i = - \left(H^{new} \frac{u^{new} - u^*}{\Delta t} + g H^{new} S_f(H^{new}, u^*) u^{new} - (\nu_t^* H^{new} u_x^{new})_x \right)_i^m \\ J_i^m = \frac{H_i^{new}}{\Delta t} + g H_i^{new} S_f(H_i^{new}, u_i^*) + \frac{(\nu_t H^{new})_{i+1/2} + (\nu_t H^{new})_{i-1/2}}{\Delta x^2} \end{aligned}$$

with $H_{i\pm 1/2}^{new}$ arithmetic averaged values, and with $(u^{new})^0 = u^*$. Unless otherwise stated, the number of relaxation iterations in the results discussed later has been set to 5.

Other aspects of the discretizations are related to the modifications of the mass fluxes, velocities, and bathymetry source terms near wet/dry interfaces. Firstly, as in [63], two cut-off values for H are introduced, one to identify dry cells (or nodes), the other to mark as troubled cells (or nodes) in which the division by H may lead to unphysical values of the velocity. To preserve well balancedness in cells containing a dry node, adverse bathymetry gradients are limited as suggested in [16] (see also [63]). In troubled cells (or nodes) instead, the mass flux is set to zero, as well as the velocities, and the dispersive corrections \mathbf{S}_d in (1), the second order terms in (2) and (13), and ψ in (5). The van-Albada slope limiter is used only in breaking regions, and only if the hybrid approach is chosen.

4 Wave breaking closure

Boussinesq equations are unable to describe both the overturning of waves, and the dissipation of kinetic energy originated during wave breaking. A physical closure is necessary. Generally, this closure consists

of two main steps. The first one is a trigger mechanism allowing to localize in space and time the initiation and the termination of breaking. The second one is a mechanism introducing a dissipation of total energy in the model. This paper focuses on two techniques to define the second element, which are discussed in some detail in the following sections. In both cases, the triggering of wave breaking is done following the criteria proposed [39, 24] which have been found simple and robust. The idea is to introduce a flagging strategy based on the following conditions:

- the surface variation criterion: a cell is flagged if $|\eta_t| \geq \gamma\sqrt{gH}$, with $\gamma \in [0.3, 0.65]$ depending on the type of breaker;
- the local slope angle criterion: a cell is flagged if $\|\nabla\eta\| \geq \tan\varphi_c$, with critical angle $\varphi_c \in [15^\circ, 30^\circ]$ depending on the flow configuration.

The first criterion is usually active in correspondence of moving waves and has the advantage of being completely local. The second criterion acts in a complementary manner, and allows to detect stationary or slow-moving hydraulic jumps [68, 39]. Flagged cells are grouped to form a breaking region. This region is either enlarged to account for the typical roller length, as suggested in [78, 39], or deactivated, depending on the value of the Froude number $Fr^2 = H_{\max}(H_{\max} + H_{\min})/(2H_{\min}^2)$, defined starting from the minimum and maximum wave height in the flagged zone. The interested reader can refer to [78, 39, 6] and references therein for more details regarding the implementation of these detection criteria.

4.1 Hybrid wave breaking model

This closure attempts to exploit the properties of hyperbolic conservation laws embedded with an entropy inequality. For the shallow water equations, in particular, the mathematical entropy coincides with the total energy [33, 74, 75]. While conserved in smooth regions, entropy/total energy is dissipated in discontinuous weak solutions, thus providing a possible candidate for the wave breaking closure. This approach is in itself neat and simple. It has the limitation that the form of the dissipation is fixed by that determined by the shallow-water Rankine-Hugoniot jump conditions, and given by (see e.g. [62] chapter 1.6, and [9])

$$\mathcal{D}_{sw} = g\sqrt{g\frac{H_{\max} + H_{\min}}{2H_{\max}H_{\min}}}\frac{(H_{\max} - H_{\min})^3}{4} \quad (14)$$

This is however a parameter free definition of the dissipation which has been proved to reproduce quite well the large scale decay of the total energy in for several types of breaking waves, and with several different underlying propagation models and relative numerical discretizations [79, 80, 70, 39, 48, 6, 44, 24]. The implementation of this closure is somewhat trivial once the wave detection algorithm discussed earlier has been properly set up. For the Nwogu's equations, it boils down to locally turning off in the whole flagged region the dispersive source \mathbf{S}_d and the second order derivative terms in (13) when evaluating the new nodal velocities. Similarly, for the GN system, the nodal values of ψ in (5) are set to zero in the breaking region.

The most limiting aspect of this approach is the switch between the non-hydrostatic and the hydrostatic equations. What has been reported by many authors in a more or less marked way, is the difficulty of performing this switch in a stable manner. Unless coarse grids are considered, with eventually the addition of local regularization numerical dissipation terms, several authors have reported the appearance of strong oscillations [70, 39, 24, 20]. These artefacts tend to become stronger and stronger as the mesh is refined. To our knowledge, there are no studies in literature reporting fully grid converged solutions with this approach due to this problem. An exception to this is perhaps one result reported in [70] showing some convergence (on only 3 grids) of the time averaged wave heights and setup, even though increasing oscillations in the local profiles are reported for the same test. This behaviour clearly poses a limitation in terms of potential for local automatic adaptation of the mesh, and its investigation is one of the objectives of this article.

4.2 Wave breaking closure via a PDE based TKE model

The use of an eddy viscosity model to provide the dissipation required for the breaking closure is one of the earliest approaches [94]. The definition of this artificial viscosity is the key of this approach, as well as the way in which it enters the Boussinesq equations. One of the most common approaches, due to Kennedy and collaborators [41] (see also [68, 39, 52] and references therein), involves a definition of the eddy viscosity based essentially on the variation in time of the free surface elevation. This term is then embedded in a viscous flux, as e.g. in (1) and (5). There exist improved variants of this idea, either also embedding some notion of vertical (along the depth) kinematics or vorticity transport [12], or attempting at improving the behavior of the total energy dissipation by also including a water elevation dissipation [18], up to more complex approaches including partial differential equations for an average turbulent kinetic energy [29, 95], or even multilayer approaches embedding PDEs for a turbulent layer flowing on top and interacting with the bulk of the wave, well representative of spilling flows [14, 53, 59, 64, 27]. In this work, we have chosen to focus our attention on an intermediate complexity approach: a wave breaking closure based on a one equation PDE for the Turbulent Kinetic Energy (TKE).

Several turbulence models exist [61, 65, 90], but very few of them have been used in a Boussinesq-type setting. Up to the authors knowledge a first approach has been proposed by Nwogu [29] who used a standard TKE model to describe the spatial and temporal evolution of the turbulent kinetic energy produced by wave breaking while solving the fully non-linear equations of Wei et al. [89]. A highly non-linear Boussinesq model with the same turbulence wave breaking model of Nwogu, has been used by Elnaggar and Watanabe [23]. More recent related works are those of Briganti et al. [12] in which a Boussinesq model is coupled with a vorticity transport equation, as well as the work of Zang et al. [95] in which they use a Green-Naghdi system with an eddy viscosity PDE derived from the TKE model. Here we propose a version of the model proposed by Nwogu modified according to some of the definitions proposed in [95], and embedding the detection criteria discussed in the beginning of this section.

Following [61, 95], the eddy viscosity is determined from the amount of the turbulent kinetic energy k , produced by the wave breaking, and a turbulent length scale ℓ_t :

$$v_t = C_\nu \sqrt{k} \ell_t \quad (15)$$

In $k - kL$ turbulence models [58, 1] (see also [95]), the constant C_ν is usually set to $C_\nu = (0.09)^{1/4} \approx 0.55$ which is the value used here. We now need a model for the computation of k and ℓ_t . Differently from the models discussed in [58, 1], here we adopt a one equation approach in which only one PDE is solved for k , while the for ℓ_t , inspired by the definition used in [95], we use a vertical average mixing length defined as

$$\ell_t = \kappa H$$

where κ is a constant controlling the width and intensity of the breaking. Concerning turbulent kinetic energy, it can be shown that in three space dimensions the following transport equations holds [61]

$$k_t + \mathbf{u} \cdot \nabla k = \mathcal{D} + \mathcal{P} - \mathcal{E} \quad (16)$$

with \mathcal{D} , \mathcal{P} , and \mathcal{E} , diffusion, production and dissipation (or destruction) terms respectively. Definitions and possible expressions of these quantities in terms of mean flow quantities can be found e.g. in the book [61]. When coupling (16) with a depth averaged Boussinesq model, several approximations are possible. Here we will combine some of the elements suggested in [29] and in [95] in order to obtain a model simple to implement, to be compared to the hybrid approach. First of all, we will assume that both k (and hence ν_t) and its transport dynamics are constant along the depth, so that (16) can be replaced by a zero-th order approximation involving only depth averaged quantities, namely

$$(Hk)_t + (Huk)_x = H\overline{\mathcal{D}} + H\overline{\mathcal{P}} + H\overline{\mathcal{E}}. \quad (17)$$

For the definition of the terms on the right hand side of (17) we have followed [29]. In particular, we have for the diffusion and destruction terms

$$H\overline{D} = H\sigma\nu_t k_{xx}, \quad H\overline{E} = -HC_D \frac{k^{3/2}}{\ell_t} \quad (18)$$

where, following [29, 95], we have set $C_D = C_\nu^3$. The constant σ allows to control the smoothness of the TKE, and hence of the breking viscosity, in the breaking region. Concerning the production term, the model used is again the one suggested in [29] assuming this quantity to depend on the vertical gradient of the velocity at the free surface. Following the notation of (16), and denoting the velocity at the free surface by $\mathbf{u}^s = \mathbf{u}(t, x, y, z = \eta)$, we have

$$H\overline{P} = HB(t, x) \mu_{\mathcal{P}} \mathbf{u}_z^s \cdot \mathbf{u}_z^s$$

As in [29], the turbulent viscosity $\mu_{\mathcal{P}}$ appearing in the production term is defined based on a mixing length hypothesis assuming a balance between production and dissipation, namely

$$\mu_{\mathcal{P}} = \frac{\ell_t^2}{\sqrt{C_D}} \sqrt{\mathbf{u}_z^s \cdot \mathbf{u}_z^s}$$

so that we end with

$$H\overline{P} = HB(t, x) \frac{\ell_t^2}{\sqrt{C_D}} (\mathbf{u}_z^s \cdot \mathbf{u}_z^s)^{3/2}. \quad (19)$$

In [29] the parameter B is equal to 0 or 1 depending on a wave breaking criterion. In the reference the criterion used is based on the ratio between the free surface velocity and the wave celerity being larger than one. Here, for simplicity B is set to one in the breaking regions detected exactly as discussed in the beginning of section §4. This also allows to detect wave breaking in the same way for the TKE and hybrid approach. Having fixed the values of C_ν and C_D , the only ‘‘tunable’’ parameters are κ and σ .

Lastly, we need to be able to evaluate the depth averaged and free surface velocities for both Boussinesq models, as well as the value of the vertical gradient of the velocity at the free surface. For this we use the vertical asymptotic development underlying the two models. In the weakly nonlinear case, this development can be used to write the following relations [60, 47]

$$u(z) = u^a - \left(\frac{z^2}{2} - \frac{d^2}{6} \right) u_{xx}^a - \left(z + \frac{d}{2} \right) (du^a)_{xx}$$

giving the free surface vertical gradient

$$u_z^s = -\eta u_{xx}^a - (du^a)_{xx}. \quad (20)$$

and the depth averaged (within the asymptotic accuracy) velocity required for the transport term in (17)

$$u = u^a + \left(\frac{(z^a)^2}{2} - \frac{d^2}{6} \right) u_{xx}^a + \left(z^a + \frac{d}{2} \right) (du^a)_{xx} \quad (21)$$

The GN equations directly provide a value of the depth averaged speed, while the fully nonlinear asymptotic development allows to write

$$u(z) = u - \left[\frac{z^2}{2} - \left(\frac{H^2}{6} - \frac{H(H-d)}{2} \right) \right] u_{xx} - \left[z - \left(\frac{H}{2} - d \right) \right] (du)_{xx}$$

which yields a similar expression for the vertical gradient of the free surface velocity, this time in function of the depth averaged velocity u :

$$u_z^s = -\eta u_{xx} - (du)_{xx}. \quad (22)$$

The fully discrete distribution of the nodal values of the TKE is obtained by integrating equation (17) with a semi implicit approach. Before the predictor step (10) is applied to the Boussinesq models, the nodal TKEs are evolved by first applying an explicit Euler update involving a third order MUSCL upwind discretisation of the transport operator $(Huk)_x$, essentially the same presented in section §3 for the shallow water equations. To avoid spurious negative values in this phase, the min-mod limiter is applied [50]. The predicted values k_i^* are then corrected by means of diagonally semi-implicit relaxation iterations similar to those used for the breaking dissipation and reading

$$\left(\frac{\Delta x}{\Delta t} + \frac{2\sigma v_{t,i}^n}{\Delta x}\right)(k_i^{m+1} - k_i^m) = \Delta x \frac{k_i^m - k_i^*}{\Delta t} + \sigma v_{t,i}^n \frac{k_{i+1}^m - 2k_i^m + k_{i-1}^m}{\Delta x} + \left(\frac{B\ell_{t,i}^2}{\sqrt{C_D}}(u_z^s)_i^{3/2}\right)^n - C_D \left(\frac{k_i^{3/2}}{\ell_{t,i}}\right)^n$$

with an initial condition, $k^0 = k^*$. For the benchmarks discussed in the paper, 4 or 5 relaxation iterations are used unless otherwise stated. Where necessary, depth average velocity (for the Nwogu model) and velocity gradient at the free surface (for both Boussinesq models) are obtained by a second order central finite difference approximation of (21), (20), and (22).

5 Boundary condition and the internal source function

In this work we use two types of boundary conditions : solid (reflective) wall and absorbing boundary conditions. For the wall boundary conditions ghost cells are used with mirrored states for the velocities, as discussed in [37]. Absorbing boundaries are used for outgoing waves. In this case, an adsorbing layer is introduced within which surface elevation and the momentum are damped by multiplying their values by a coefficient $m(x)$ defined as [39]

$$m(x) = \sqrt{1 - \left(\frac{d(x)}{L_s}\right)^2} \quad (23)$$

where L_s is the sponge layer width, and $d(x)$ is the distance from the end of the absorbing boundary. As prescribed in [39], the width L_s should depend on the wavelength of the outgoing wave. For a given wavelength L , the sponge layer width should be $L \leq L_s \leq 1.5L$.

Concerning wave generation, we follow the approach of Wei et al. [88]. To obtain a desired oscillation signal in the wave generating area, a source function $S(\mathbf{x}, t)$ is added into the mass conservation equation at each time step, which is expressed as

$$S(\mathbf{x}, t) = D^* \exp(\gamma(x - x_s)^2) \sin(-\omega t) \quad (24)$$

in which

$$\gamma = \frac{5}{(\delta L/4)^2} = \frac{80}{\delta^2 L^2} \quad (25)$$

where L is the wave length, ω the wave frequency, θ the wave incident angle, x_s is the location of the center of the wave-making area, δ is a parameter that influences the width $W = \delta L/2$ of the wave generator area and D^* is the source function's amplitude. For a monochromatic wave, D^* is defined as

$$D^* = \frac{2\sqrt{\gamma}A_0(\omega^2 - \alpha_1 g k^4 h^3)}{\omega k \sqrt{\pi} \exp(-l^2/4\gamma) [1 - \alpha(kh)^2]} \quad (26)$$

where h is the still water level at the wave generation region, A_0 the wave amplitude, $l(= k_x)$ the wave number in the x -direction, $\alpha = -0.390$ and $\alpha_1 = \alpha + 1/3$.

For multi-chromatic waves following [30] we use linear superposition. According to the irregular wave concept of Longuet and Higgings (1961) the water surface elevation can be described by

$$\eta(t) = \sum_{i=1}^{\text{inf}} a_i \cos(\omega_i t + \epsilon_i)$$

where, a_i and ω_i represent the amplitude and frequency of the component wave respectively and ϵ_i denotes the initial phase of the component wave. This means that each component wave has its deterministic amplitude and frequency. The source function now is:

$$S(\mathbf{x}, t) = \exp(\gamma(x - x_s)^2) \sum_{i=1}^M D_i^* \sin(-\omega_i t + \epsilon_i) \quad (27)$$

where each component has an amplitude of

$$D_i^* = \frac{2\sqrt{\gamma}A_i(\omega_i^2 - \alpha_1 g k_i^4 h^3)}{\omega k_i \sqrt{\pi} \exp(-k_i^2/4\gamma) [1 - \alpha(k_i h)^2]}. \quad (28)$$

To determine the width of the wave making area, we use the maximum wavelength between the components.

6 Numerical results

6.1 Wave breaking over a bar

This test case of Beji and Battjes [7] examines the sinusoidal wave propagation over a submerged bar. The scope of this test case is to investigate the frequency dispersion characteristic and non-linear interaction of complex wave propagation phenomena. A sketch of the problem is provided in figure 2. The computational domain is $x \in [0, 35m]$, with sponge layers placed at both ends. Periodic waves were generated at $x = 10m$ over a mean water depth of $0.4m$. Wave height and period are set to $a = 0.054m$, and $T = 2.5s$, corresponding to a dispersion parameter $kh \approx 0.52$. Waves propagate over submerged trapezoidal bar with a toe at $x = 15m$, a front slope of 1 : 20, a $2m$ long plateau of $0.3m$ height, and a lee slope of 1 : 10. More informations on the experiment can be found in [7] and in the references using this test case for model validation [24, 39, 46, 78].

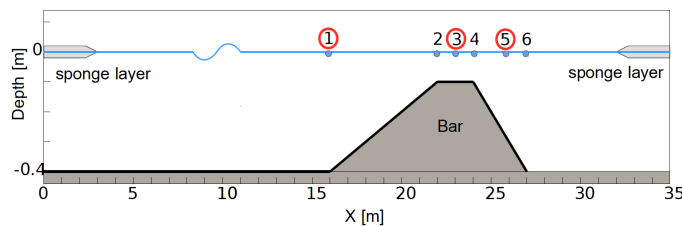


Figure 2: Wave breaking over a bar: problem sketch, and position of the gauges

Concerning the model parameters, for this highly unsteady problem the surface variation detection parameter γ (cf. section §4) is the one more sensitive to the onset of breaking. For the computations

performed here we have set $\gamma = 0.3$. The parameters used for the TKE are not the same for the two Boussinesq propagation models. In particular, we have set $\kappa_{GN} = 2.8$ and $\sigma_{GN} = 1.2$ for the GN equations, while $\kappa_N = 3.2$ and $\sigma_N = 1.2$ for the Nwogu system.

Experimental data are available in several wave gauges placed before, on top, and after the bar. Here we focus on three gauges (cf. figure 2) placed before the toe of the bar, gauge 1 at $x = 16m$, on top of the plateau, gauge 3 at $x = 23m$, and on the lee slope, gauge 5 at $x = 26m$. We will discuss numerical results obtained on three different meshes of size $4cm$, $2cm$, and $1cm$. For the Nwogu model, we could not run the hybrid breaking simulations on the last mesh due to instabilities at the Boussinesq-shallow water interface. Similarly, when using the hybrid approach we could not go below $\Delta x = 1cm$ when using the GN model for propagation. Note also that the results discussed here are those obtained after a transient of 36 seconds, differently from what is done e.g. in [24, 39], where the four first waves are analyzed. The results are presented in figures 3, 5 and 6, for gauges 1,3, and 5, respectively.

Figure 3 allows to visualize the behaviour of the models at the toe of the bar, right at the end of the wave propagation region. This gauge allows to highlight the initial asymmetry of the waves, essentially due to the interaction with the submerged bar. Some preliminary observations can be made. Firstly, the fully nonlinear model (left column) seems to capture better the shape of the waves, the weakly nonlinear one providing a signal which is slightly too peaky. Secondly, we see already at this stage that while the TKE model (blue curves) shows little sensitivity to the mesh size, the signals obtained with the hybrid approach (green curves) depend strongly on this parameter. We can clearly see on the intermediate and fine mesh (in the GN case) higher frequency components absent in the TKE results. These components are generated in correspondence of the boundary of the wave breaking region, as it can be clearly seen in the snapshots of figure 4. These instabilities become stronger as the mesh is refined, and may ultimately lead to the blow up of the solution, as it is the case for the Nwogu model on the fines mesh, and of the GN model on finer meshes.

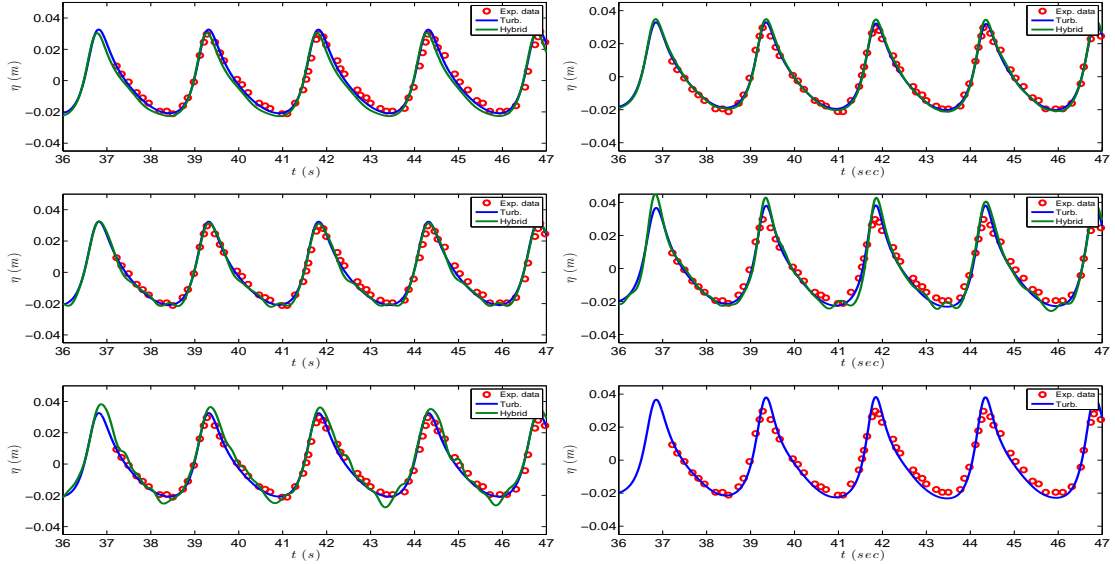


Figure 3: Time series of surface elevation at wave gauge 1 for the GN (left) and Nwogu (right) models using the TKE (blue) and Hybrid (green) wave breaking closure.

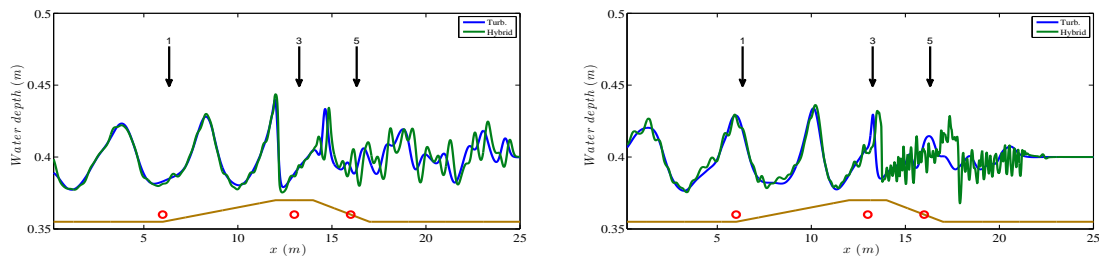


Figure 4: Snapshots of the flow for the GN (left) and Nwogu (right) models using the TKE (blue) and Hybrid (green) wave breaking closure.

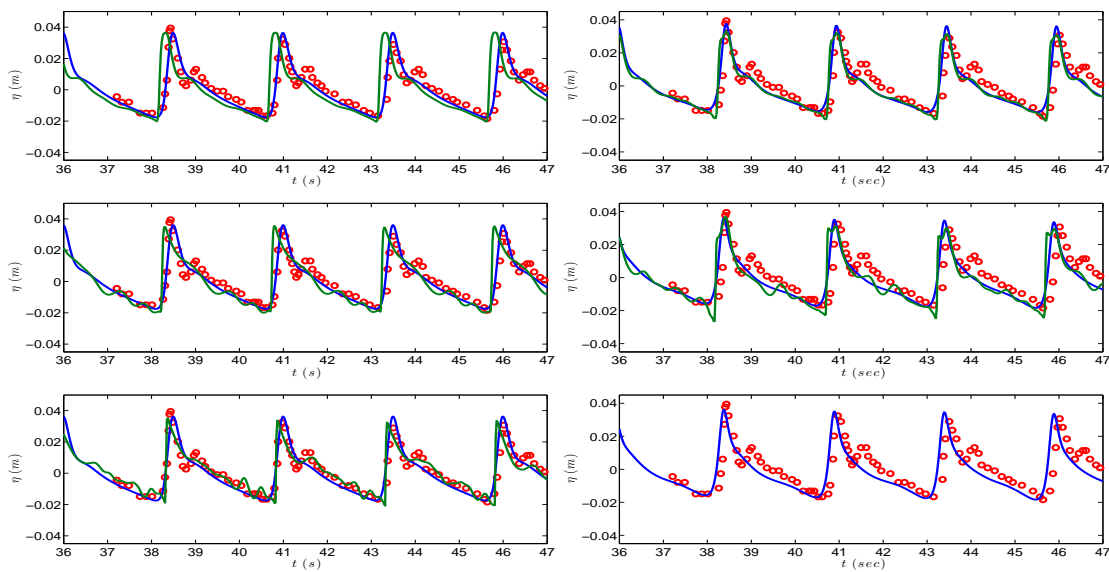


Figure 5: Time series of surface elevation at wave gauge 3 for the GN (left) and Nwogu (right) models using the TKE (blue) and Hybrid (green) wave breaking closure.

Figures 5 and 6 confirm the preliminary observations made for the first gauge. In particular we can clearly see the strong dependence of the results of the hybrid model on the mesh size. For this approach we can also see how the breaking waves are represented as very sharp fronts. For the GN model, on the coarse mesh breaking stops early enough for the signal in these two gauges to be smooth. This however leads to a noticeable phase lag. As the mesh is refined, the waves break more strongly. This leads clearly to an improvement on the phase. This behaviour curiously is not observed for the Nwogu model which shows strong and sharp breaking fronts already on the coarsest mesh level, with a correct phase. This allows to highlight the need of tailoring the choice of the breaking detection criterion to the propagation model. Here the same parameters have been used for both. Nevertheless, both set of results allow to visually see the appearance of spurious higher frequencies in the signal. These are the result of the coupling between the dispersive and non-dispersive regions. For the weakly non-linear model (right column) we can see the inception of the instability already on the medium resolution used here in figure 6. This is less evident for the GN model, which still provides numerical solutions on the finer level used. We were however unable to refine once more the mesh without solution blow up.

The TKE approach is clearly less sensitive, at least for this test, to both the choice of the model parametrization, and the mesh size. This is summarized in figure 7, showing a grid convergence for the gauge 3. We also would like to remark that, for Nwogu's equations and for plunging breakers, Demirblik and Nwogu in [19] resorted to a more complex TKE closure with a PDE for the B coefficient in the production term (19). We found out that the simplified formulation adopted here, combined with the physical criteria for the initiation and termination of the process discussed in the beginning of section §4 can simulate reasonably well plunging wave breakers.

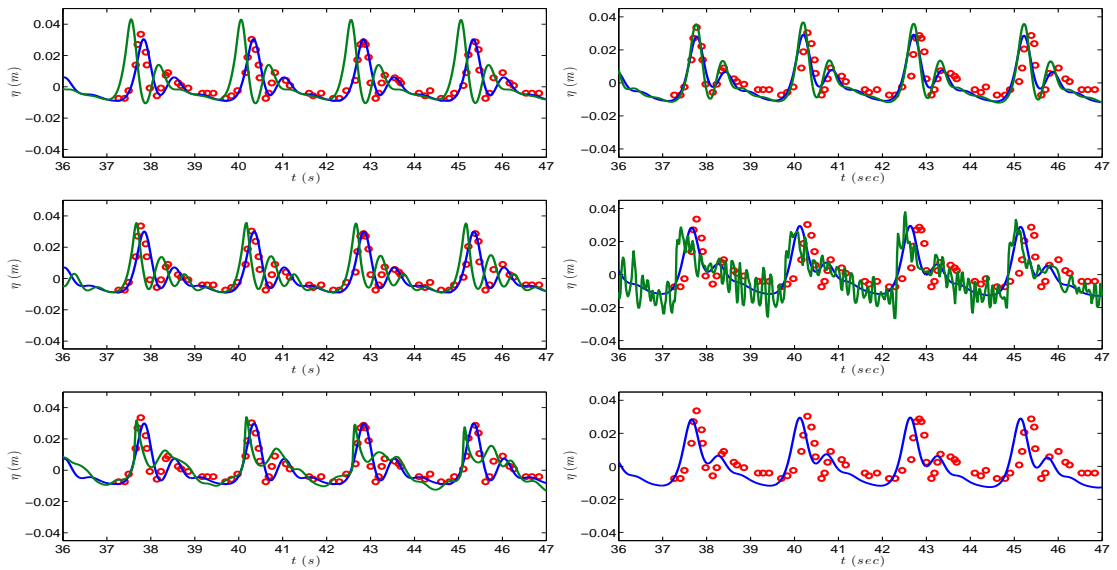


Figure 6: Time series of surface elevation at wave gauge 5 for the GN (left) and Nwogu (right) models using the TKE (blue) and Hybrid (green) wave breaking closure.

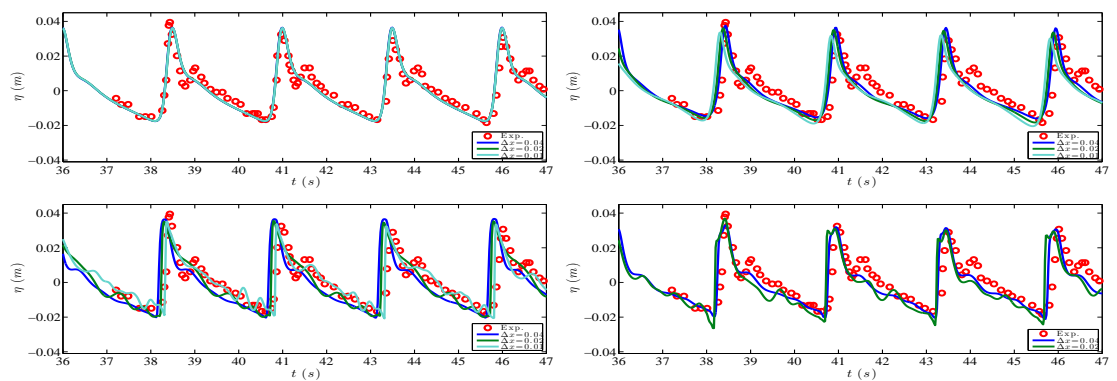


Figure 7: Time series of surface elevation at wave gauge 3 for different mesh size. For the GN (left) and Nwogu (right) models using the TKE (up) and Hybrid (down) wave breaking closure.

6.2 Solitary waves breaking on a slope

One of the most intensively studied problems in long wave modelling is the solitary wave run-up on a plane beach, see for example [73, 4, 39, 80, 94, 68, 17] among others. In this test case we want to study propagation, breaking and run-up of a solitary wave over a planar beach with a slope 1 : 19.85. With this famous test case we assess the ability of our model to describe shoreline motions and wave breaking when it occurs. The incident wave height considered in this case is $A/d = 0.28$ with $d = 1$, so according to Synolakis [73] the wave breaks strongly both in the run-up and in the rundown phase of the motion. The GN and Nwogu's equations are tested and compared, using for each one the turbulent kinetic energy wave breaking model and the hybrid wave breaking model. The same holds for all the test cases that follows.

The computation domain is of $120m$, where $x \in [-20, 100]$. The CFL used is 0.3 and sponge layer was applied off-shore with length $L_s = 5m$. A Manning coefficient of $n_m = 0.01$ was used to define the glass surface roughness used in the experiments. As before, computations have been run on three different meshes with size $\Delta x = [0.025, 0.0125, 0.0063m]$. The parameters of the wave breaking criteria used in this test case are $\gamma = 0.6$ and $\phi_c = 30^\circ$ for both models. To properly capture the hydraulic jump generated at during backwash, the TKE parameters depend here both on the propagation model and on the type of breaking criterion satisfied. In particular, for unsteady waves the surface time variation criterion is the one activated. In this case we use $\kappa_{GN} = 0.75$, $\sigma_{GN} = 0.9$ for the GN model and $\kappa_N = 0.8$, $\sigma_N = 1.5$ for Nwogu's model. If the slope criterion is activated, we use instead higher values, namely we set $\kappa_{GN} = 1.5$, $\sigma_{GN} = 15.5$ and $\kappa_N = 1.5$, $\sigma_N = 1.5$.

Figure 8 compares the numerical surface profiles for the GN equations and the experimental measurements. The same is plotted for Nwogu's equations in figure 9. The numerical solution was obtained using $\Delta x = 0.05m$. As expected, both mathematical models produced similar behaviour. Until time $t\sqrt{g/h} = 10$ the solitary propagates to the shore and the two wave breaking models produce, as expected, identical results since wave breaking hasn't started yet. As expected the Nwogu's model gives a wave which overshoots and breaks slightly earlier compared to the one produced by the GN equations. The experimental wave breaks around $t\sqrt{g/h} = 20$. The numerical solution for the hybrid model is represented like a bore storing the water spilled from the breaking wave behind the front. At time $t\sqrt{g/h} = 20$ the turbulence model represents the solution as a triangular bore considerably closer to the experimental data than the hybrid one. Similar behaviour has been observed by other researchers that used eddy viscosity models [41, 68, 94]. At time $t\sqrt{g/h} = 25$ the bore collapses at the shore, and both approaches show good qualitative agreement with the data. After that the wave starts to run-up, with a maximum run-up occurring at $t\sqrt{g/h} = 45$. As the water recedes, a breaking wave is created near the still water level. The numerical solution is approximated as a hydraulic jump for both numerical models. It is fully resolved using both breaking models, since the breaking criterion recognises the hydraulic jump and the NSW equations are used for the hybrid model while the proper amount of viscosity is added by the turbulent kinetic energy model.

Figures 10 and 11 show the numerical results for both breaking phases (at time $t\sqrt{g/h} = 20$ and $t\sqrt{g/h} = 60$ respectively) while refining the mesh. Up to the authors knowledge it is the first time that such a study is performed for a (quasi-)steady hydraulic jump for an eddy viscosity type model. The first set of figures depict the breaking of the wave which travels on-shore for both GN (left column) and Nwogu equations (right column). We can clearly see the oscillatory nature of the mean. However this is completely spoiled by the oscillations produced due to the switching between the two sets of equations. On the contrary the turbulent kinetic energy wave breaking mechanism remains stable and gives a convergent solution for both sets of equations. The second set of figures plot the same for the hydraulic jump formed at backwash. The difference between the two approaches is more accentuated here. It is quite hard to see a convergence for the hybrid results, while this is clearly the case for the TKE ones. We must mention that the GN equations combined with the hybrid model is blowing up after

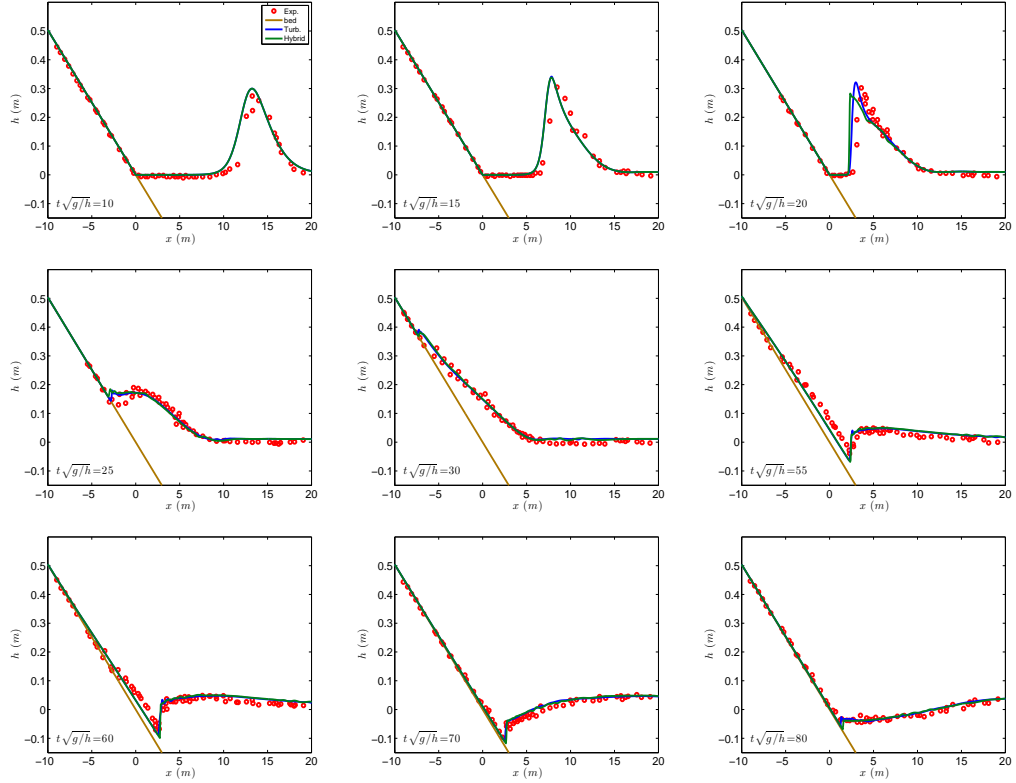


Figure 8: Free surface elevation of solitary wave run-up on a plane beach for the GN model.

$t\sqrt{g}/h = 60$ for $\Delta x = 0.0063$, while Nwogu's equations are more sensitive to the hybrid formulation since numerical solution is obtained only for the first two meshes.

At last, we have repeated this test for a more non-linear initial wave with $\epsilon = 0.5$, on the mesh with $\Delta x = 0.025m$. The results obtained at incipient breaking before the runup and during backwash are reported on figure 12. As before the hybrid mechanism produces oscillations, in both breakers, and it is very unstable for Nwogu model. Oscillations are clearly visible for the GN results with the hybrid breaking. Smooth capturing of the breakers is obtained also in this case with the TKE model. Figures 13 and 14 show again, the numerical results for both breaking phases while refining the meshes for the turbulent kinetic energy mechanism. The Hybrid closure is not converging since the oscillatory nature of the mechanism is more pronounced in this case.

6.3 Wave height and setup prediction

The analysis of [9] shows that wave setup is very sensitive to the dissipation mechanism in wave breaking. To investigate this aspect we consider two of the experiments performed by Hansen and Svendsen [31]. These experimental studies consider several different regular waves shoaling and breaking on a sloping beach. Many authors have used these tests to validate their models and the associated breaking closures [41, 80, 39, 70, 18].

We consider here two cases, one involving a spilling breaker, the second involving a plunging breaker. Regular waves are generated over a $0.36m$ horizontal bottom, propagated shoaled and broke over a slope

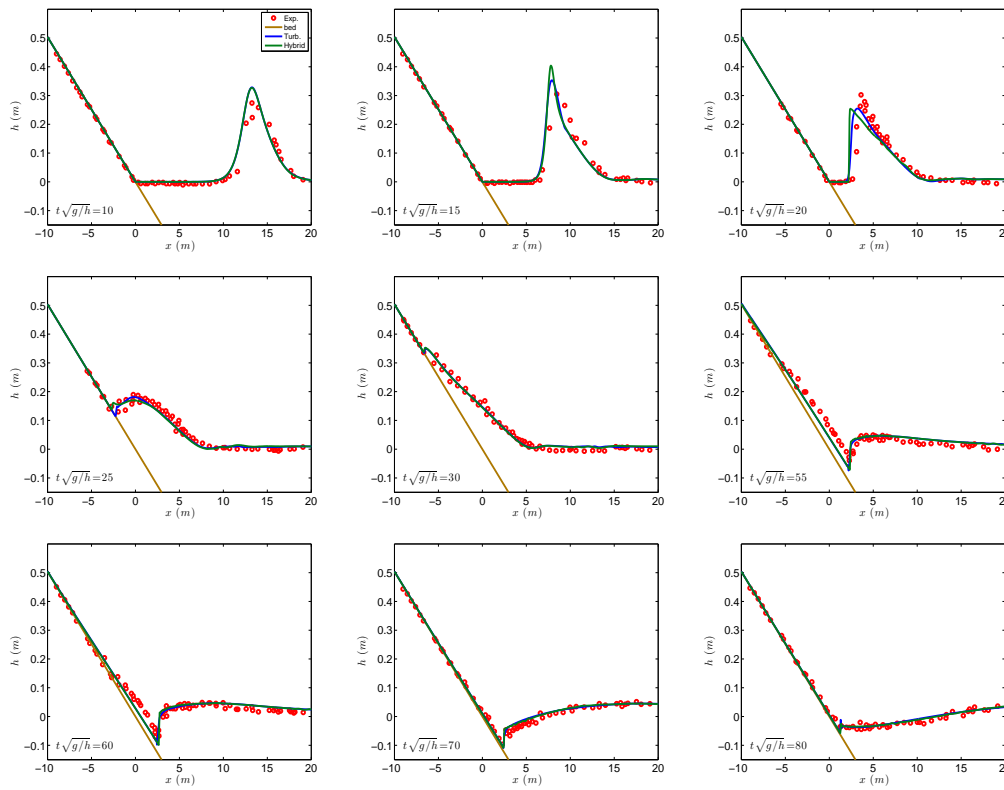


Figure 9: Free surface elevation of solitary wave run-up on a plane beach for Nwogu’s model.

of 1 : 32.26. In the spilling breaking case (test number 05041) the regular wave’s period T is 2.0s, and the wave’s height H is 0.036m. The second test case (test number 03041) is a strong plunging breaking case with $T = 3.33s$ and $H = 0.043m$. The tests have been run on a 52m long domain $x \in [-26 \ 26]$, discretised with cells of $\Delta x = 0.02m$, and with $CFL = 0.3$. A sponge layer is applied offshore with length $L_s = 5m$. The wave making internal source was placed 14.78m offshore from the toe of the beach, and bottom friction is neglected. The free surface elevation, recorded at wave gauges which placed every 0.1m., is analysed to compute the mean wave height, and the position of the mean water level (MWL). The value of γ in the surface variation criterion equals to 0.5 for both models. Concerning the wave breaking closures, we have set $\kappa_{GN} = 0.8$, $\sigma_{GN} = 0.05$ and $\kappa_N = 0.8$, $\sigma_N = 0.4$, for the two GN and Nwogu models respectively.

The numerical results obtained for the two cases considered are reported on figures 15 and 16, in terms of wave height (left) and mean water level (right). As before, the blue lines in the figures refer to the TKE results, while the green ones to the hybrid wave breaking, and the top row report the computations of the GN model, while the bottom ones the results of the Nwogu equations.

For the spilling case, figure 15 seems to indicate that in all cases the detection criterion provides an early breaking. This of course alters the strength of the numerical breaking, which is less intense. This translates in a wave height decrease slower than the experimental one. Even so, the computations compare reasonably well with the experiments, especially when compared with results in the published literature [41, 80, 39, 70, 18]. This is confirmed by the mean water level plots. Although we can clearly observe

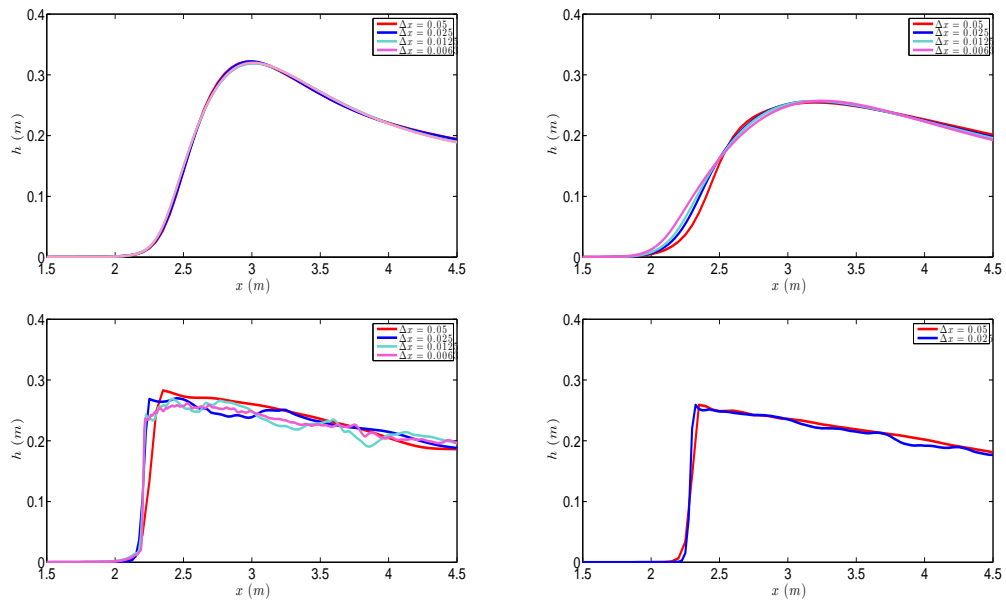


Figure 10: Breaking bore on different meshes for the GN (left) and Nwogu's (right) models, using the TKE (up) and the hybrid (down) wave breaking closure.

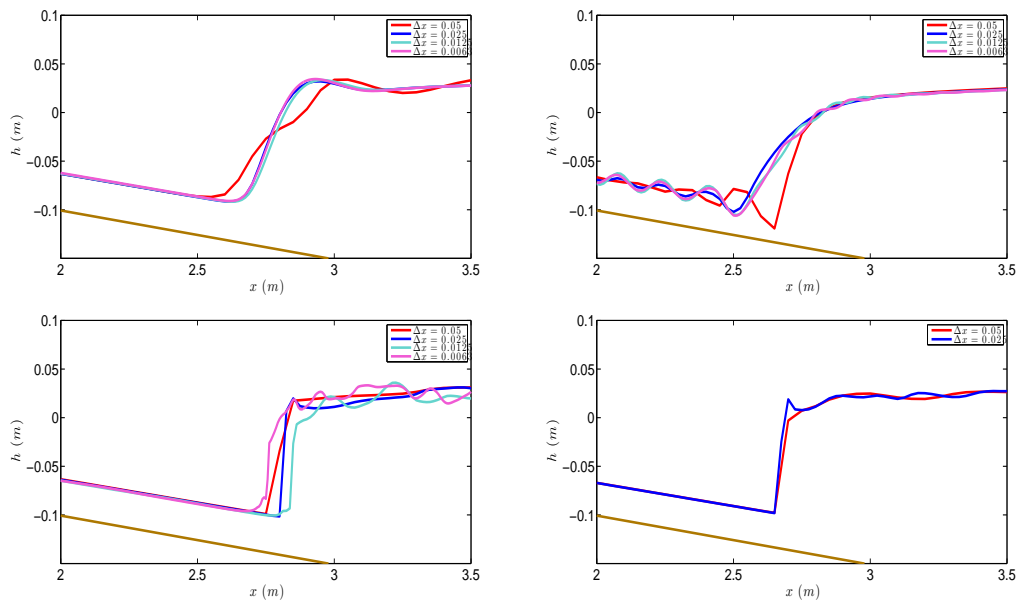


Figure 11: Hydraulic jump on different meshes for the GN (left) and Nwogu's (right) models, using the TKE (up) and the hybrid (down) wave breaking closure.

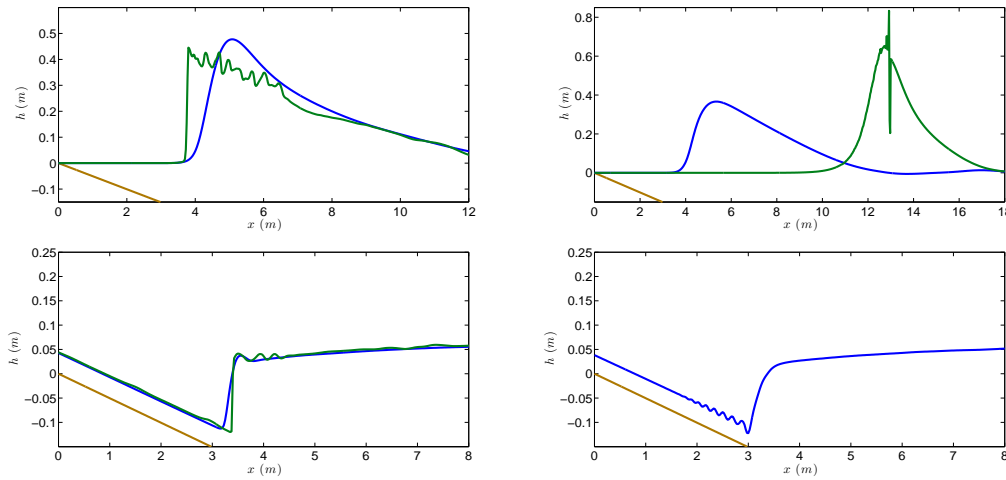


Figure 12: Breaking in the run-up (up) and the run-down (down) phase for GN (left) and Nwogu’s equations (right) for $\epsilon = 0.5$, using the TKE (blue) and the hybrid (green) wave breaking closure.

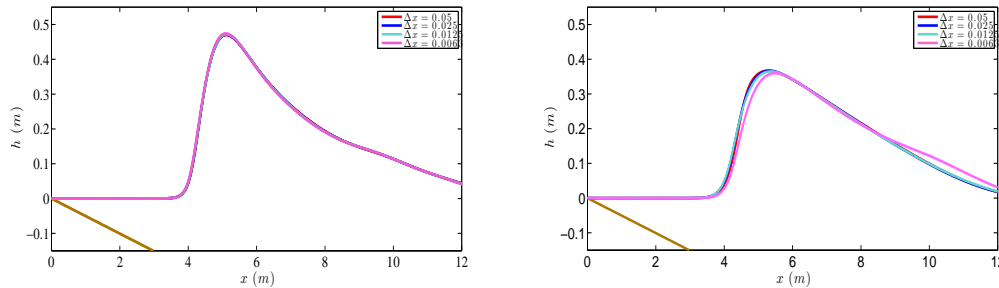


Figure 13: Breaking bore on different meshes for the GN (left) and Nwogu’s (right) models for $\epsilon = 0.5$, using the TKE (up) and the hybrid (down) wave breaking closure.

the early start of setup, due to the early breaking, the slopes of the numerical signals are quite close to those of the experimental ones. According to the analysis of [9] this shows that the amount of dissipation introduced is correct. We stress that the differences between the TKE and hybrid approach are minor, even though we tend to consider the results obtained with the turbulence model slightly better in terms of both wave height and slope of the setup.

For the plunging case, figure 16, the agreement with the experimental values is even better. We can see that the breaking location is detected correctly in this case, even though both the GN and the Nwogu model provide an underestimation of the shoaling with both breaking closures. The wave height decrease is predicted with a slightly smaller slope, but the agreement with the data is quite satisfactory. The setup prediction is very good, with both location of the breaker and slope reproduced correctly by all models.

Some conclusions can be drawn from the implementation of this numerical test case. The first one is that both wave breaking closures allow to detect and handle both spilling and plunging breaking of regular waves. We stress that the parametrisation used for TKE closure is the same for the two cases considered.

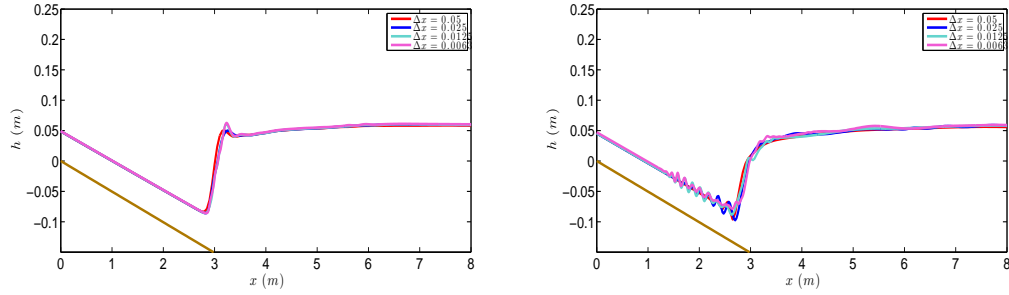


Figure 14: Hydraulic jump on different meshes for the GN (left) and Nwogu's (right) models for $\epsilon = 0.5$, using the TKE (up) and the hybrid (down) wave breaking closure.

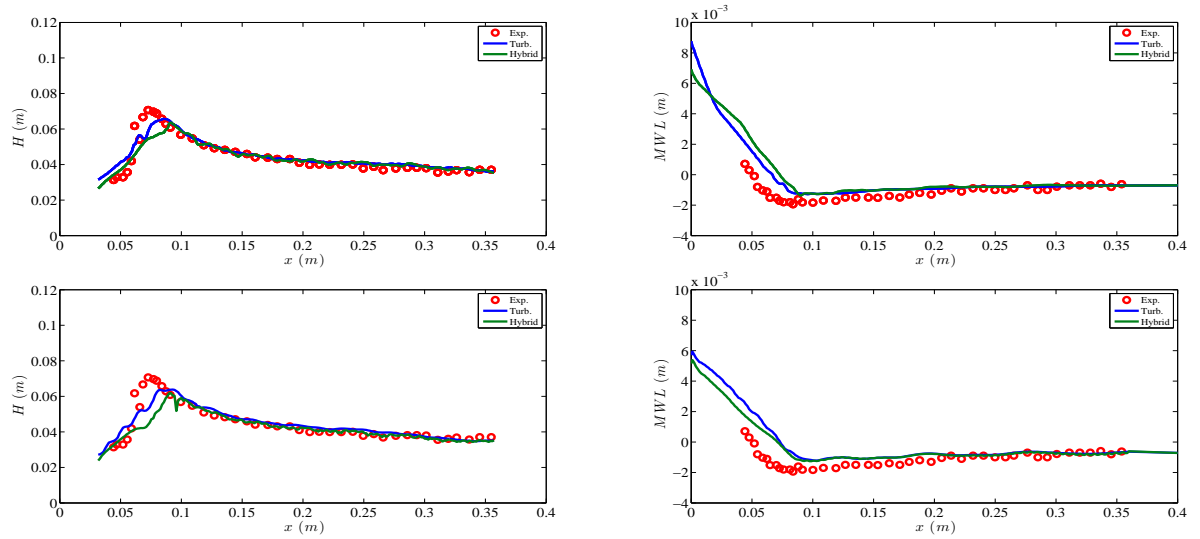


Figure 15: Computed and measured wave heights (left) and set-up (right) using equations. Test number 05041 (spilling breaking). Top: GN equations. Bottom: Nwogu equations.

This shows the potential of this type of approach to provide a robust accurate energy dissipation rate, independently on the number of nodal points per wavelength, and on the nonlinearity of the problem.

6.4 Breaking of a dichromatic wave train

Mase [56] performed a number of experimental test cases to the study shoaling, breaking and runup of various types of dichromatic wave trains on mild slopes. Here we want to compare the two breaking closures studied for the wave pattern described by

$$\eta(t) = a_1 \cos(2\pi f_1 t) + a_1 \cos(2\pi f_2 t) \quad (29)$$

with $f_1 = 1.05f_m$ and $f_2 = 0.95f_m$, $a_1 = 0.15cm$ is the wave amplitude, which corresponds to the medium energy level experiment in [56]. Here, we consider the case with mean frequency $f_m = 0.6Hz$. The pattern of the wave train consists of ten individual waves. To simulate this pattern, we have used the

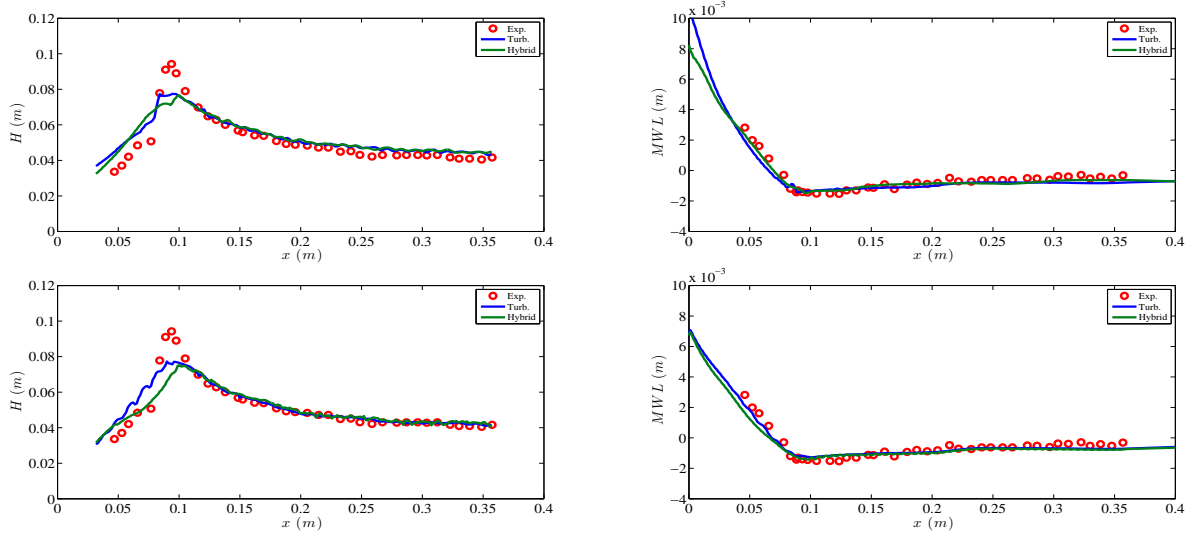


Figure 16: Computed and measured wave heights (left) and set-up (right) using equations. Test number 03041 (plunging breaking). Top: GN equations. Bottom: Nwogu equations.

40m long numerical domain $x \in [-15, 25]$. Waves were generated internally at $x = 0m$, propagated on a flat bottom for 10m. A mild slope of 1 : 20 starts at $x = 10m$, over which the waves shoal and break. A sponge layer of $L_s = 8m$ was placed on both boundaries. We have run this case on one mesh, with size $\Delta x = 0.02m$, and using a $CFL = 0.3$. The surface variation criterion was used for the detection of the breaking waves with a parameter γ of 0.35. For the TKE closure $\kappa_{GN} = 0.75$, $\sigma_{GN} = 0.8$ and $\kappa_N = 2.5$, $\sigma_N = 3.5$. Data exist for wave gauges placed at $x = 10m$ (WG1), $x = 16.9m$ (WG8), $x = 17.9m$ (WG10) and $x = 18.9m$ (WG12), measuring the free surface elevation in time.

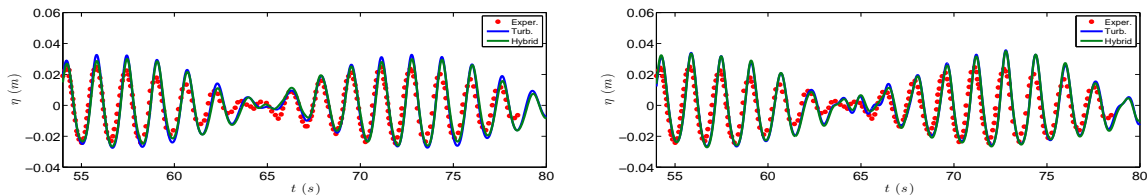


Figure 17: Dichromatic waves: surface elevation at gauge WG1. Left: GN equations. Right: Nwogu equations.

We refer to [56, 82, 54] for more informations concerning this benchmark, and others of the same family. In particular, we mention that according to [82] in the experiments the generation of spurious harmonics was not compensated at the generator and there was no active absorption of the reflected waves, therefore it is difficult to reproduce the laboratory conditions exactly. Furthermore, the measured frequencies and amplitudes deviated slightly from the target. Different approaches have been used as to obtain numerically the desired signal. Here we follow the approach proposed in [82] where it is suggested to use a mean frequency slightly different the nominal one, adjusting it so that the correct frequency is obtained at the toe of the beach. This "frequency calibration" has led here to the signals displayed in figure 17m obtained by setting $f_m = 0.61Hz$.

The waves have been let shoal and break on the 1 : 20 slope. We evaluate the profiles obtained in the

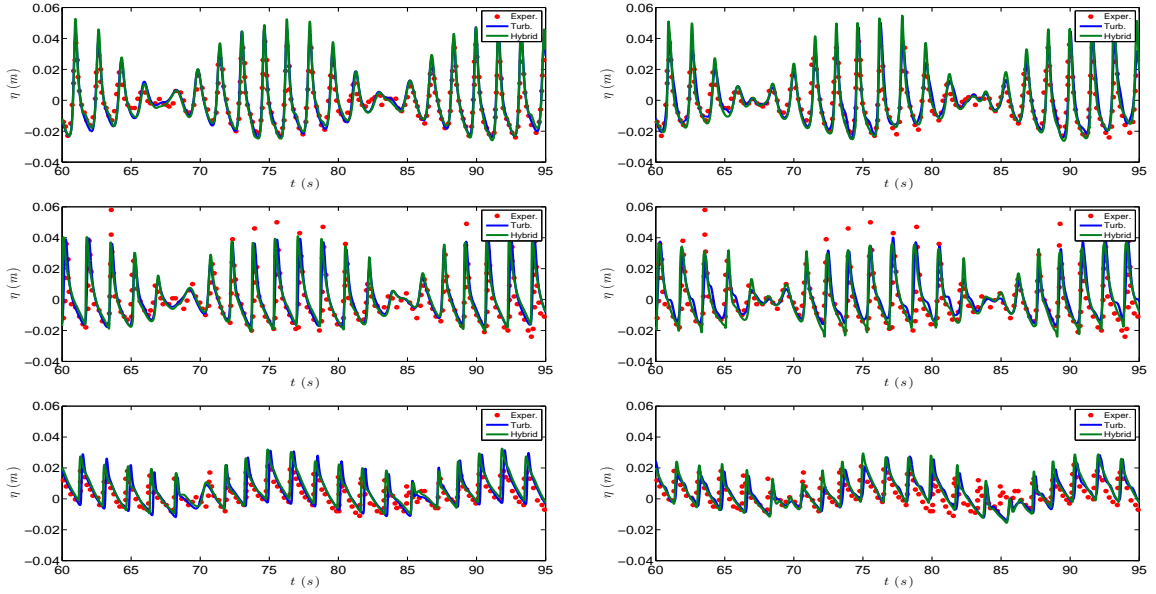


Figure 18: Dichromatic waves: surface elevation at gauges WG8 (top), WG10 (middle) and WG12 (bottom). Left: GN equations. Right: Nwogu equations.

downstream gauges on figure 18, where the left column reports the results obtained with the GN model, and the right one those obtained with Nwogu’s equations. For this problem, and on this mesh resolution, both models, as well both wave breaking closures, provide a reasonably accurate prediction of the wave transformation, as well as of the decay of the wave height.

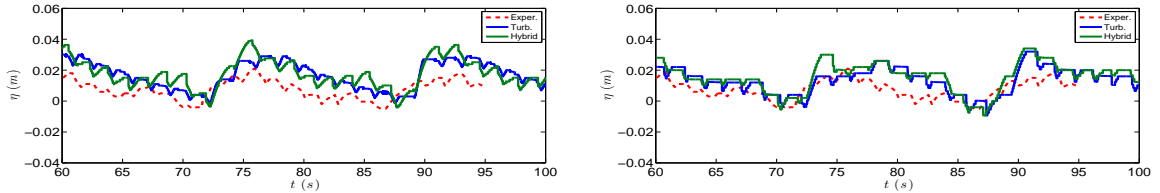


Figure 19: Dichromatic waves: shoreline displacement for the GN (left) and Nwogu model (right).

Finally, figure 19 presents the shoreline displacement for the two sets of equations. The main remarks that could be made here are that the fully nonlinear model allows a better description of the non-symmetric movement of the shoreline, with runups faster than the backwashes. Also, the TKE closure provides a smoother signal, the hybrid approach giving some over-shooting levels of the wet line.

6.5 Propagation, breaking, and overtopping of a 2D reef

This next test case is reported as a complex application in order to show the potential of the modelling choices evaluated here to handle the interaction of the whole range of phenomena: dispersive propagation, shoaling, breaking, overtopping, reflection. The benchmark considered was initially proposed in [67, 68], and later used by several authors for validation [68, 81, 24, 40]. The problem involves a bathymetry consisting of a reef with a fore slope of 1/12 and a crest of 0.2m reef crest and an offshore water depth

of $2.5m$. The reef crest is exposed by $0.06m$ and hides on the lee side a flat with a depth of $0.14m$. Water height distributions at several time instants and water height time series in 14 wave gauges have been measured in the flume experiments at Oregon State University within the PhD work of V. Roeber [67] (see also [68]). A sketch of the reef geometry, showing the positioning of the wave gauges, is reported in figure 20. The initial state consists of a solitary wave of amplitude $a = 0.75m$ which propagates onshore, shoals and breaks in front of the reef crest. Walls are present at both ends of the domain. We refer to [67, 68] for a more detailed description of the experimental and computational setup. Our results have been computed on a mesh with size $\Delta x = 0.05$, and setting $CFL = 0.3$. Manning friction has been used, with a Manning coefficient $n_m = 0.012$. Both wave breaking detection criteria are used with $\gamma = 0.6$ and $\phi_c = 30^\circ$. Concerning the TKE closure $\kappa_{GN} = 0.75$, $\sigma_{GN} = 0.8$ and $\kappa_N = 1.2$, $\sigma_N = 1.5$ but when a hydraulic jump is detected the values are set to $\kappa_{GN} = 1.5$, $\sigma_{GN} = 15.5$ and $\kappa_N = 3.5$, $\sigma_N = 16$.

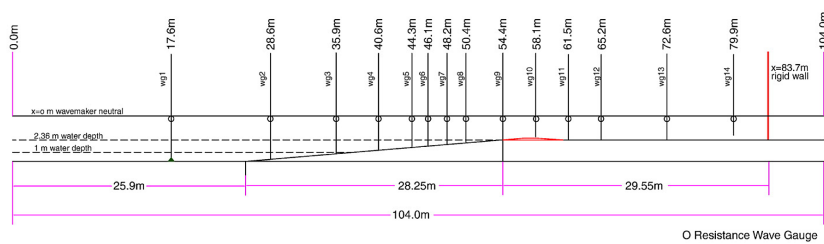


Figure 20: 2D reef geometry and wave gauge locations

To visualise the results we group snapshots of the free surface in three phases : propagation and shoaling of the initial soliton (figure 21); overtopping and formation, propagation and reflection of a bores on the lee side of the reef (figure 22); secondary overtopping, with formation of a quasi-steady hydraulic jump and of an undular bore (figure 23). In all the figures, the top rows report the results obtained with the GN model, the bottom rows refer to the results of the Nwogu model, the blue lines are those obtained with the TKE breaking model, and the green lines are those of the hybrid breaking treatment. Symbols refer to the experimental values provided in [67].

The figures show that all models allow, on this mesh resolution, a quite satisfactory prediction of the water height. The differences between different choices appear to be minor. We can mention that, at least in our implementation both the fully and the weakly nonlinear models tend to predict the moving bores on the lee side with some phase advance. This, at least in our implementation, is more pronounced for the fully nonlinear GN mode, as we can see e.g. on figure 22 (central and right column). This behaviour is independent on the breaking closure adopted. We can also remark that when using the hybrid wave breaking with the Nwogu equations some over-prediction of the amplitude of the undulating bores is observed.

To have some more insight in the capabilities of the models, we analyze the water height time series in gauges WG5, WG9, WG10, and WG12. The plots are reported on figures 24 and 25. The dispersive propagation of the waves is visible in WG5 and, at for the fore side undulating bores, in WG9. We can see that all the models capture correctly the shoaling of the initial solitary, and that despite a visible phase lag, provide a quite reasonable amplitude and frequency of the undulating bores on the fore side, as it can be seen e.g. in the WG5 series on figure 24, for times larger than $70s$, and in WG9 after $80s$. In WG5 we can see again the over-amplification of the amplitude of the undular bores for the Nwogu model with hybrid wave breaking.

Concerning breaking, we can see the first breaker approximation very well reproduced from the WG9 series at time around $34.5s$. The hydraulic jump forming at $55s$ is also well reproduced in amplitude, albeit with a phase advance. Similar observations can be made when looking at figure 25. The WG12

results, in particular, show an excellent agreement for the first four bores. All the models give an under-prediction of the water level behind the slowly moving hydraulic jump which forms behind the main right-going bore (time $\approx 38s$). The first reflected bore at time roughly $50s$, as well as the second hydraulic jump forming after the second overtopping (time $\approx 60s$) are also very well captured by the models. The later reflections present instead a visible phase error, albeit correct in amplitude. Lastly, the WG10 results in the same figure show a nice capturing of the first two overtopping phases, although an over-prediction of the water height is also observed. The later overtoppings are affected by a phase advance already mentioned for the bores responsible for them.

Overall we consider the results quite good for all the models. Some of the differences w.r.t. the experimental water heights we are convinced that are also due to the definition of this quantity in presence of air entrainment at the free surface, as it was the case for the experimental breakers. We stress very strongly that with the current implementation the simple TKE breaking closure can handle without any problem simultaneous breakers of different types, and of different intensities. For this test, as for all the others analyzed in the paper, the fully nonlinear GN model with TKE closure provides the most robust combination.

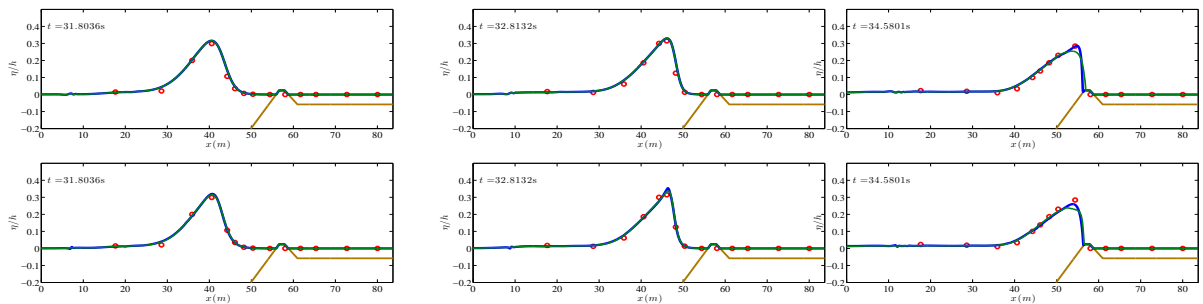


Figure 21: Overtopping of a 2D reef. Propagation, shoaling, and overtopping phases. Top row: GN model. Bottom row: Nwogu model. Blue lines: TKE breaking closure. Green Lines: hybrid wave breaking closure.

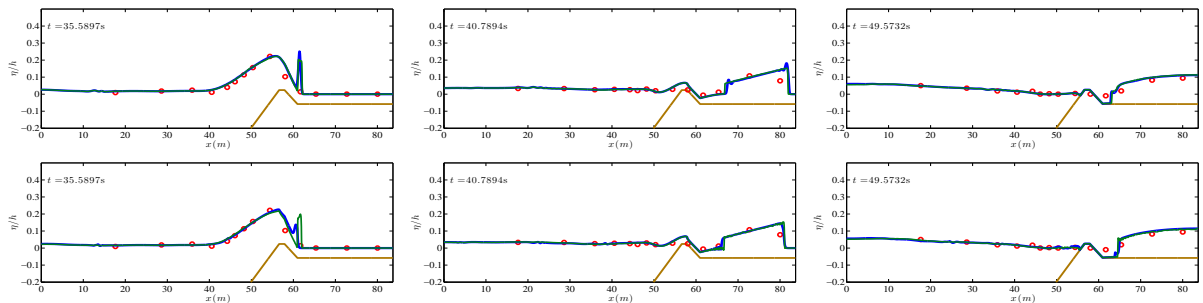


Figure 22: Overtopping of a 2D reef. Bore formation and propagation behind the reef. Top row: GN model. Bottom row: Nwogu model. Blue lines: TKE breaking closure. Green Lines: hybrid wave breaking closure.

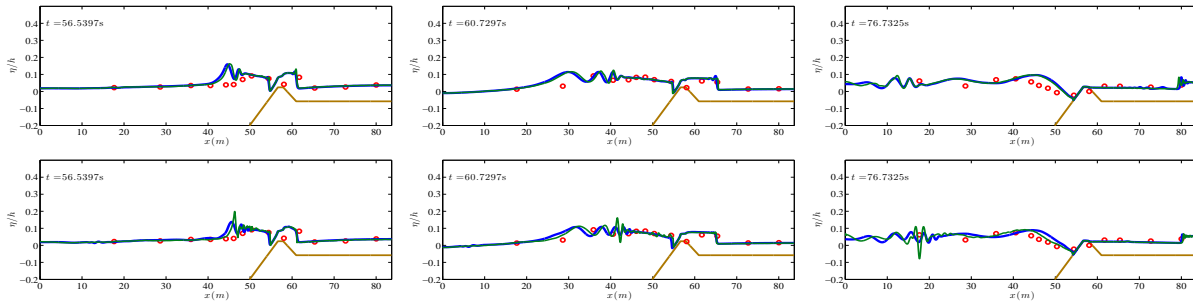


Figure 23: Overtopping of a 2D reef. Second overtopping and undular bore formation. Top row: GN model. Bottom row: Nwogu model. Blue lines: TKE breaking closure. Green Lines: hybrid wave breaking closure.

6.6 Breaking bore propagation and energy dissipation

We consider in this test case the propagation of a breaking bore over a flat bottom and we examine the energy dissipation produced by the breaking mechanisms used and the numerical scheme. The initial step which transforms to a bore can be defined by

$$\begin{cases} h(x, 0) = \frac{1}{2}(d_b - d_a)(1 - \tanh \frac{x}{a}) + d_a \\ u(x, 0) = \frac{1}{2}(u_b - u_a)(1 - \tanh \frac{x}{a}) + u_a, \end{cases} \quad (30)$$

where d_a and d_b are the water depth in front and behind the bore, u_a and u_b the corresponding depth-averaged velocities. In our case $u_a = 0$, $d_a = 1m$ and $a = 2m$. For each Froude number (F_r), u_b and d_b are computed, solving the mass and momentum conservation conditions across the bore. For $F_r > 1.4$ the initial step evolves into a breaking bore. More informations on the test case can be found in [77] and references therein.

The computational domain used is $x \in [-150, 150]$, $CFL = 0.2$ and $\Delta x = 0.1$. For this type of wave the parameter most sensitive to the onset of breaking is the time derivative of the elevation γ , which we have set here to $\gamma = 0.4$. For the turbulence model we have used $\kappa_{GN} = \kappa_N = 1.5$, $\sigma_{GN} = \sigma_N = 0.8$ for the GN and Nwogu equations respectively. Figure 26 shows the propagated bore at $t = 0, 1, 15s$ for the two models for a Froude number $F_r = 2$. The bore is breaking as it propagates through the channel, and a slightly different behaviour is observed for the two breaking closures. Hybrid breaking provides a travelling shock, for both propagation models, while the turbulent closure presents a more diffusive behaviour, with a small overshoot before the bore for the GN model.

This lends itself to a quantitative evaluation of the dissipation introduced by the different components of our numerical model. We stress very strongly that a proper evaluation of such quantity would require first of all the use of PDE models for which some clear energy conservation statement can be derived, as well as of schemes which are compatible with such a statement. While the GN equations do have a total energy which may be used for this purpose, this is not the case for Nowgu's model for which, one can at best derive approximate conservation [47, 2]. We also stress that the discretizations employed has no exact energy/entropy stability properties. For these issues, we refer to [47, 2, 57] and references therein, concerning the PDE continuous modelling, and to [76, 26, 91] and references therein, for aspects related to the energy stable approximation of the shallow water equations. The construction of exactly energy preserving schemes for dispersive equations is still a subject of research, the interested reader may refer to [84, 35, 93, 92] for some recent results concerning dispersive equations.

To provide some quantitative evaluation of the modelling closures proposed, we use here a simpler

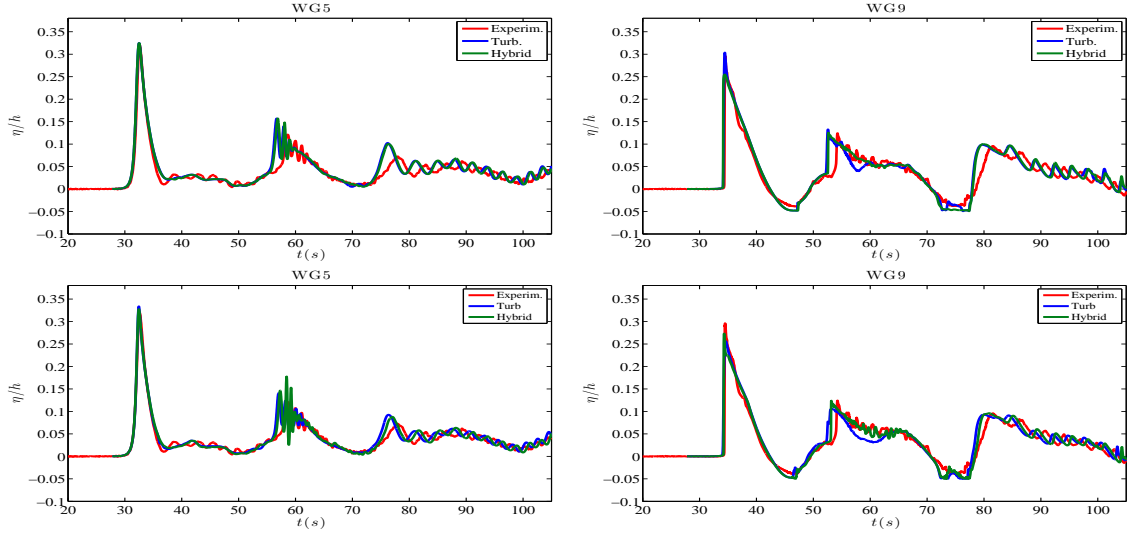


Figure 24: Overtopping of a 2D reef. Free surface time series in wave gauges WG5 (left) and WG9 (right). Top row: GN model. Bottom row: Nwogu model. Blue lines: TKE breaking closure. Green Lines: hybrid wave breaking closure.

strategy: we compare the dissipation of the shallow water energy introduced by the upwinding terms of the finite volume scheme (12), with those of the eddy viscosity term. To evaluate these quantities we have used the standard relation between the total shallow water energy E and the shallow water fluxes \mathbf{F} , namely (see e.g. [74, 75, 76])

$$\partial_t E \approx -\mathbf{V}^t (\nabla \cdot \mathbf{F} + \mathbf{S})$$

with \mathbf{V} the array of energy variables $\mathbf{V}^t = [g(H+b) - u^2/2, u]$. Given the discrete solutions at different time levels t^n , we have then computed the following quantity (cf equation (12)) related to the energy removal due to upwinding in the interval $[t^n, t^{n+1}]$:

$$D_{up}^{n+1/2} = \sum_{j \geq 1} \left\{ \mathbf{v}_{j+1/2}^t \left(\frac{1}{2} |\mathbf{A}|_{j+1/2} \Delta_{j+1/2} \mathbf{U} + \frac{gH_{j+1/2}}{2} \text{sign}(\mathbf{A})_{j+1/2} \Delta_{j+1/2} [0, b]^t \right) \right\}^{n+1/2},$$

where the last term is the upwind contribution of the bathymetry source. Note that the evaluation of the above quantity the right hand side contributions are assembled on the fly during the computation. This means that the limiters eventually active in the shallow water shocks are take into account. Similarly, we have computed the following quantity related to the energy removal due to the eddy viscosity term in the interval $[t^n, t^{n+1}]$:

$$D_{\nu}^{n+1/2} = \sum_{j \geq 1} \left\{ \nu_{t,j+1/2} H_{j+1/2} (\Delta_{j+1/2} u)^2 \right\}^{n+1/2}.$$

These terms evolve during the transformation of the solution into a bore, as shown on figure 26, and quickly converge to a steady value, which is plotted in figures 27 and 28 against the shallow water dissipation (14), for different Froude numbers and on different meshes. For the GN model, and for the range of Froude numbers tested, the TKE dissipation is within 10-15% of the value predicted by (14), while the upwind terms basically provide a negligible contribution. Conversely, these terms are, when using the hybrid approach, within 6% of (14). This shows that, when using the TKE model the numerical dissipation does not contribute to the breaking process. It also shows that the two closure models provide

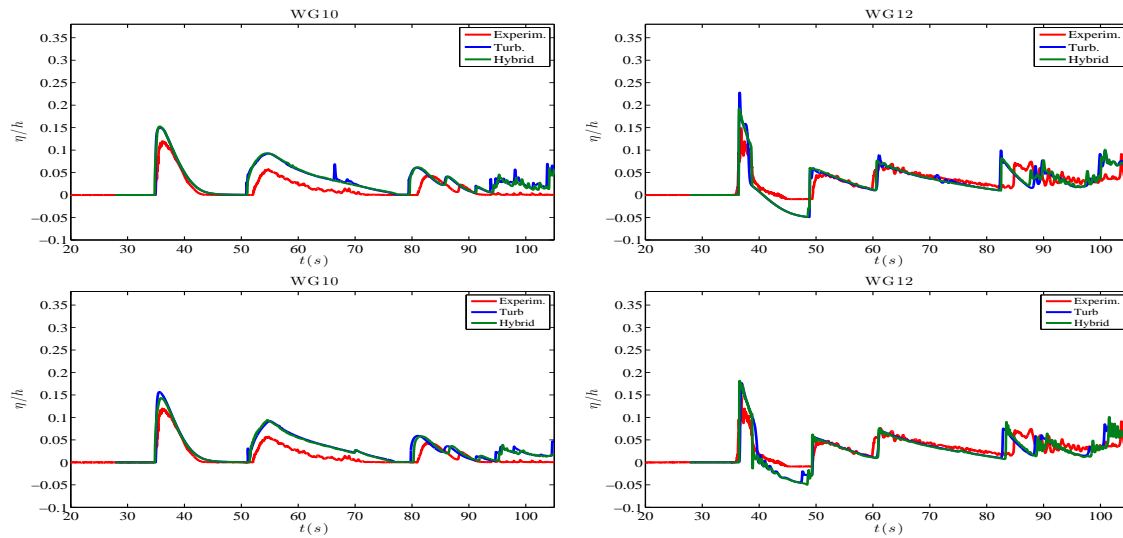


Figure 25: Overtopping of a 2D reef. Free surface time series in wave gauges WG10 (left) and WG12 (right). Top row: GN model. Bottom row: Nwogu model. Blue lines: TKE breaking closure. Green Lines: hybrid wave breaking closure.

quantitatively similar dissipation, and corroborates the results on the other benchmarks. Note that for this case both approaches provide stable results as the mesh is refined, as clear from the pictures on figure 27. Similar conclusions can be drawn for the Nwogu model by looking at figure 28. Also in this case when using the TKE closure the numerical dissipation is orders of magnitude smaller than that related to the eddy viscosity. In this case the difference between the dissipative effects obtained with the two closures is more pronounced, but the order of magnitude remains the same.

7 Conclusions

We have considered the issue of modelling wave breaking in conjunction with Boussinesq near shore propagation models. We have in particular focused on the breaking closure of a weakly nonlinear/weakly dispersive model based on the classical enhanced equations of Nwogu [60], as well as of a fully nonlinear/weakly dispersive model using the Green-Naghdi system in the form proposed in [10, 24]. We have performed a one-to-one comparison of an eddy viscosity type model, using a PDE for a turbulent kinetic energy to define the viscosity, with the hybrid approach consisting in neglecting dispersive terms in breaking regions.

The results discussed indicate that, at least with the (rather standard) implementation proposed here both closure approaches allow to describe correctly wave transformation and breaking at large scales. We have also shown that the energy dissipation introduced by the two approaches in the model is comparable, and that, for moderate Froude numbers (from 1.5 to above 2.2) it is of the same order of magnitude described by the classical hydraulics formula (14). We have shown that when using the TKE approach the numerical dissipation is way smaller than that of the closure, and thus does not contribute to the breaking process. The TKE approach, has been systematically shown to be more robust, and much less dependent on the mesh size. The use of adaptive mesh refinement seems out of the question for the moment when using the hybrid approach. The robustness of the TKE closure is particularly evident when using fully nonlinear propagation, which also seems to consistently provide an improved description of

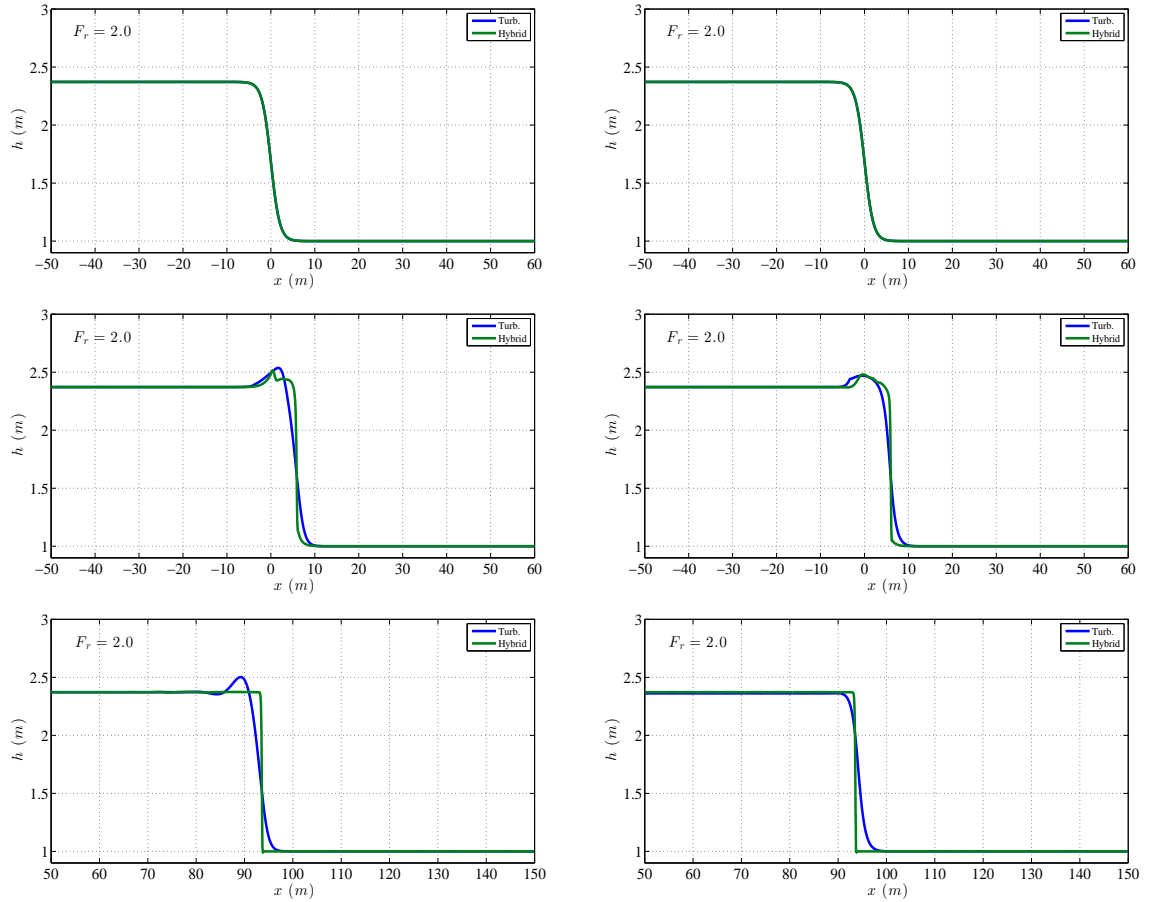


Figure 26: Free surface profiles at $t = 0, 1, 15$ s of hydraulic bores with $Fr = 2.0$. Left: GN model. Right: Nwogu model.

the wave shapes, and positions.

This preliminary study would benefit from further investigation using both improved numerics (e.g. energy preserving approximations in the propagation region), as well as improved models for both the propagation and for the breaking. The models considered at the moment present a dependence on the parameters of the detection criteria, as well as on the coefficients of the TKE equation. Improved models, including the effects of vertical variations of the flow in both the propagation and breaking may be considered in future studies (see e.g. [27]). The multi-dimensional case will also have to be studied with attention. In this case more complex effects may come into the picture, related to the interaction with transversal variations of the bathymetry (see e.g. [43]). These effects, and their interaction with the breaking closure will have to be assessed systematically.

Acknowledgements

Work partially funded by the TANDEM contract, reference ANR-11-RSNR-0023-01 of the French *Programme Investissements d'Avenir*.

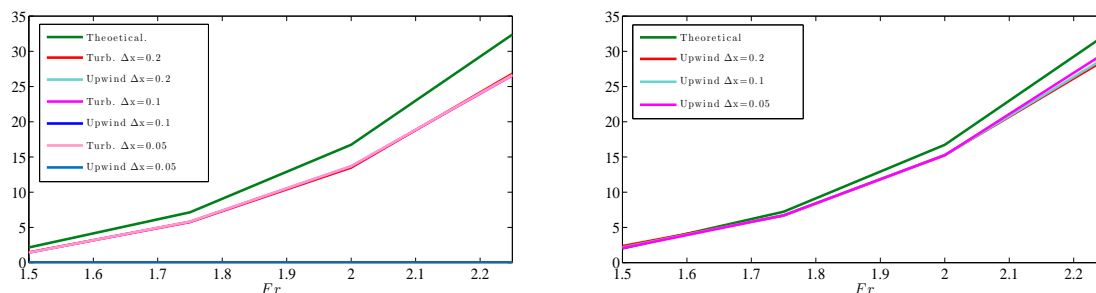


Figure 27: Energy dissipation profile for GN model using turbulent closure (left) and hybrid closure (right).

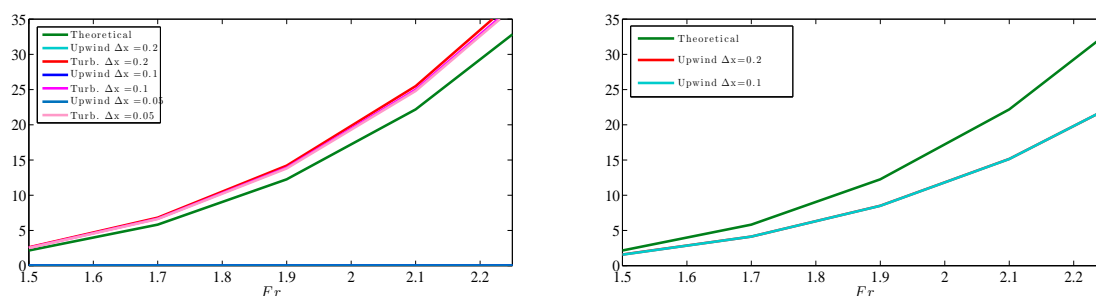


Figure 28: Energy dissipation profile for Nwogu model using turbulent closure (left) and hybrid closure (right).

References

- [1] K.S. Abdol-Hamid. Assessments of - Turbulence Model Based on Menter's Modification to Rotta's Two-Equation Model. *International Journal of Aerospace Engineering*, 2015, 2015. Article ID 987682, doi:10.1155/2015/987682.
- [2] A. Ali and H. Kalisch. Mechanical balance laws for boussinesq models of surface water waves. *Journal of Nonlinear Science*, 22(3):371–398, Jun 2012.
- [3] B. Alvarez-Samaniego and D. Lannes. A Nash-Moser theorem for singular evolution equations. Application to the Serre and Green-Naghdi equations. *Indiana University MATHematics Journal*, 57(1), 2008.
- [4] D. Arnaud and F. Marche. A discontinuous Galerkin method for a new class of Green-Naghdi equations on simplicial unstructured meshes. *Applied Mathematical Modelling*, In press.
- [5] Luca Arpaia and Mario Ricchiuto. r-adaptation for Shallow Water flows: conservation, well balancedness, efficiency. Research Report RR-8956, Inria Bordeaux Sud-Ouest, 2016. submitted to *Computers and Fluids*.
- [6] P. Bacigaluppi, M. Ricchiuto, and P. Bonneton. A 1d stabilized finite element model for non-hydrostatic wave breaking and run-up. In J. Fuhrmann, M. Ohlberger, and C. Rohde, editors, *Finite Volumes for Complex Applications VII*, volume 77 of *Springer Proceedings in Mathematics and Statistics*. Springer, 2014.

- [7] S. Beji and J. A. Battjes. Experimental investigations of wave propagation over a bar. *Coastal Eng.*, 19:151, 1993.
- [8] A. Bermudez and M.E. Vazquez. Upwind methods for hyperbolic conservation laws with source terms. *Computers & Fluids*, 23(8):1049 – 1071, 1994.
- [9] P. Bonneton. Modelling of periodic wave transformation in the inner surf zone. *Ocean Engineering*, 34(10):1459 – 1471, 2007.
- [10] P. Bonneton, F. Chazel, D. Lannes, F. Marche, and M. Tissier. A splitting approach for the fully nonlinear and weakly dispersive green-naghdi model. *Journal of Computational Physics*, 230, 2011.
- [11] A. G. L. Borthwick, M. Ford, B. P. Weston, P. H. Taylor, and P. K. Stansby. Solitary wave transformation, breaking and run-up at a beach. *Maritime Engineering*, 159:97–105, 2006.
- [12] R. Briganti, R. E. Musumeci, G. Belloti, M Brocchini, and E. Foti. Boussinesq modeling of breaking waves: Description of turbulence. *J. Geophys. Res.*, 109, 2004.
- [13] M. Brocchini. A reasoned overview on Boussinesq-type models: the interplay between physics, mathematics and numerics. *Proc. R. Soc. A*, 469 (20130496):dx.doi.org/10.1098/rspa.2013.0496, 2013.
- [14] M. Brocchini and D.H. Peregrine. The dynamics of strong turbulence at free surfaces. part 2. free-surface boundary conditions. *J. Fluid Mech.*, 449:255–290, 2001.
- [15] A. Castro and D. Lannes. Fully nonlinear long-wave models in the presence of vorticity. *J. Fluid Mech.*, 759:642–675, 2014.
- [16] M. J. Castro, A. M. Ferreiro, J. A. García-Rodríguez, J. M. González-Vida, J. Macías, C. Parés, and M. E. Vázquez-Cendón. The numerical treatment of wet/dry fronts in shallow flows: Application to one-layer and two-layer systems. *Mathematical and Computer Modelling*, 42:419–439, 2005.
- [17] R. Cienfuegos, E. Barthélemy, and P. Bonneton. A fourth-order compact finite volume scheme for fully nonlinear and weakly dispersive Boussinesq-type equations. Part II: Boundary conditions and validation. *Int. J. Numer. Methods Fluids*, 53:1423–1455, 2007.
- [18] R. Cienfuegos, E. Barthélemy, and P. Bonneton. Wave-breaking model for Boussinesq-type equations including roller effects in the mass conservation equation. *J. Waterw., Port, Coast., Ocean Engrg.*, 136:10–26, 2010.
- [19] A. Demirbilek, Z. Zundel and O. Nwogu. Boussinesq modeling of wave propagation and runup over fringing coral reefs, model evaluation report. coastal and hydraulics laboratory technical note chltr0712. vicksburg. IMS: U.S. Army Engineer Research and Development Center, 2007.
- [20] A. Duran. Tsunami propagation: Numerical issues 1. well balancedness, positivity preservation, high order of accuracy. In *TANDEM and DEFIS LITTORAL Tsunami school*, Bordeaux, France, 2016.
- [21] A. Duran and F. Marche. Discontinuous-Galerkin discretization of a new class of Green-Naghdi equations. *Communications in Computational Physics, Global Science Press*, page 130, 2014.
- [22] A. Duran, F. Marche, and Q. Liang. On the well-balanced numerical discretization of shallow water equations on unstructured meshes. *J. Comput. Phys.*, 235:565–586, 2013.

- [23] A. Elnaggar, Z. Watanabe. Nonlinear Wave Dynamics in Surf and Swash Zones. In *Proceedings 27th International Conference on Coastal Engineering*, 2000.
- [24] M. Filippini, A.G. Kazolea and M. Ricchiuto. A flexible genuinely nonlinear approach for nonlinear wave propagation, breaking and runup. *J. Comp. Phys.*, 310:381–417, 2016.
- [25] M. Filippini, A.G. Kazolea and M. Ricchiuto. A flexible genuinely nonlinear approach for nonlinear wave propagation, breaking and runup on unstructured grids. In *27th International Offshore and Polar Engineering Conference (ISOPE)*, June 2017.
- [26] U.S. Fjordholm, S. Mishra, and E. Tadmor. Well-balanced and energy stable schemes for the shallow water equations with discontinuous topography. *Journal of Computational Physics*, 230(14):5587 – 5609, 2011.
- [27] S. L. Gavriluk, V. Yu. Liapidevskii, and A. A. Chesnokov. Spilling breakers in shallow water: applications to favre waves and to the shoaling and breaking of solitary waves. *Journal of Fluid Mechanics*, 808:441–468, 2016.
- [28] A.E. Green and P. M. Naghdi. A derivation of equations for wave propagation in water of variable depth. *J. Fluid Mech.*, 78:237–246, 1976.
- [29] G. Hanbin, L. Yanbao, L. Shaowu, and Luwen Q. Numerical prediction of breaking waves and currents with a Boussinesq model. In *Proceedings 25th International Conference on Coastal Engineering*, 1996.
- [30] G. Hanbin, L. Yanbao, L. Shaowu, and Luwen Q. Applications of a boussinesq wave model. In *International Conference on Estuaries and Coasts*, 2003.
- [31] J. B. Hansen and I. A. Svendsen. Regular waves in shoaling water: experimental data. Technical Report, ISVA Series Paper 21, 1979.
- [32] A. Harten. High resolution schemes for hyperbolic conservation laws. *J. Comp. Phys.*, 49:1, 1983.
- [33] A. Harten. On the symmetric form of systems of conservation laws with entropy. *J. Comput. Phys.*, 49:151–164, 1983.
- [34] A. Harten and P. Hyman. Self-adjusting grid methods for one-dimensional hyperbolic conservation laws. *J. Comp. Phys.*, 50:235, 1983.
- [35] Chaolong Jiang, Jianqiang Sun, Xunfeng He, and Lanlan Zhou. High order energy-preserving method of the ‘good’ boussinesq equation. *Numerical Mathematics: Theory, Methods and Applications*, 9(1):111–122, 2016.
- [36] Th. V. Karambas and C. Koutitas. A breaking wave propagation model based on the Boussinesq equations. *Coastal Engineering*, 18:1–19, 1992.
- [37] M. Kazolea and A. I. Delis. A well-balanced shock-capturing hybrid finite volume-finite difference numerical scheme for extended 1D boussinesq models. *Applied Numerical Mathematics*, 67:167–186, 2013.
- [38] M. Kazolea, A. I. Delis, I. A. Nikolos, and C. E. Synolakis. An unstructured finite volume numerical scheme for extended 2D Boussinesq-type equations. *Coast. Eng.*, 69:42–66, 2012.
- [39] M. Kazolea, A. I. Delis, and C. E. Synolakis. Numerical treatment of wave breaking on unstructured finite volume approximations for extended Boussinesq-type equations. *J. Comput. Phys.*, 271:281–305, 2014.

- [40] M. Kazolea, A.G Filippini, M. Ricchiuto, A. Stéphane, M. M. Medina, D. Morichon, C. Journeau, R. Marcer, K. Pons, L. R. Sylvestre, R. Pedreros, and Rousseau M. Wave propagation breaking, and overtoping on a 2D reef : a comparative evaluation of numerical codes for tsunami modelling. Research Report RR-9005, January 2017.
- [41] A. B. Kennedy, J .T. Chen, Q. Kirby, and R. A. Dalrymple. Boussinesq modeling of wave transformation, breaking and runup. Part I: 1D. *J. Waterw., Port, Coast., Ocean Engrg.*, 126:39–47, 2000.
- [42] M. J. Kermani, A. G. Geber, and J. M. Stockie. Thermodynamically based moisture prediction using roe’s scheme. In *The 4th Conference of Iranian AeroSpace Society*, 2003. Amir Kabir University of Technology, Tehran, Iran, January.
- [43] D.I. Ketcheson and M. Quezada de Luna. Diffractons: Solitary waves created by diffraction in periodic media. *SIAM Multiscale Model. Simul.*, 13(1):440–458, 2015.
- [44] J. Kim, J. K. Pederson, F. Lovholt, and LeVeque R. J. A Boussinesq type extension of the GeoClaw model - a study of wave breaking phenomena applying dispersive long wave models. *Coastal Eng.*, 122:75–86, 2017.
- [45] J.T. Kirby. Boussinesq models and their application to coastal processes across a wide range of scales. *Journal of Waterway, Port, Coastal and Ocean Engineering*, 142(6), 2016.
- [46] G.Th. Klonaris, C.D. Memos, and Th.V. Karambas. A boussinesq-type model including wave-breaking terms in both continuity and momentum equations. *Ocean Engineering*, 57:128 – 140, 2013.
- [47] D. Lannes. *The water waves Problem, Mathematical Analysis and Asymptotics*. American Mathematical Society, Mathematical surveys and monographs, 2013.
- [48] D. Lannes and F. Marche. A new class of fully nonlinear and weakly dispersive Green-Nagdi models for efficient 2d simulations. *J. Comp. Phys.*, 282:238–268, 2015.
- [49] D. Lannes and F. Marche. Nonlinear wave-current interactions in shallow water. *Studies in applied mathematics*, 136:382–423, 2016.
- [50] R. J. LeVeque. *Finite Volume Methods for Hyperbolic Problems*. Cambridge University Press, 2002.
- [51] P. J. Lynett. Nearshore Wave Modeling with High-Order Boussinesq-Type Equations. *Journal of Waterway, Port, Coastal, and Ocean Engineering*, 132:348–357, 2006.
- [52] P. J. Lynett, T. R. Wu, and P. L. F. Liu. Modeling wave runup with depth integrated equations. *Coastal Eng.*, 46:98–107, 2002.
- [53] Brocchini M. Free surface boundary conditions at a bubbly/weakly splashing air-water interface. *Physics of fluids*, 14:1834–1840, 2002.
- [54] P.A. Madsen, O. R. Sørensen, and H. A. Schäffer. Surf zone dynamics simulated by a Boussinesq-type model: Part I. Model description and cross-shore motion of regular waves. *Coast. Eng.*, 32:255–288, 1997a.
- [55] P.A. Madsen, O. R. Sørensen, and H. A. Schäffer. Surf zone dynamics simulated by a Boussinesq-type model: Part II. Surf beat and swash oscillations for wave groups and irregular waves. *Coast. Eng.*, 32:289–319, 1997b.

- [56] H. Mase. Frequency down-shift of swash oscillations compared to incident waves. *J. Hydraulic Res*, 33:3:397–411, 1995.
- [57] Y. Matsuno. Hamiltonian structure for two-dimensional extended green–naghdi equations. *Proceedings of the Royal Society of London A: Mathematical, Physical and Engineering Sciences*, 472(2190), 2016.
- [58] F. R. Menter and Y. Egorov. The scale-adaptive simulation method for unsteady turbulent flow predictions. part 1: Theory and model description. *Flow, Turbulence and Combustion*, 85(1):113–138, 2010.
- [59] S.K. Misra, M. Brocchini, and J.T. Kirby. Turbulent interfacial boundary conditions for spilling breakers. In *Proceedings of the Coastal Engineering Conference*, 2007.
- [60] O. Nwogu. An alternative form of the Boussinesq equations for nearshore wave propagation. *Journal of Waterway, Port, Coastal, and Ocean Engineering*, 119:618–638, 1994.
- [61] S. B. Pope. *Turbulent Flows*. Cambridge University Press, Cambridge, 2003.
- [62] L.L.J. Pratt and J.A. Whitehead. *Rotating Hydraulics*, volume 36 of *Atmospheric and Oceanographic Sciences Library*. Springer-Verlag, New-York, 2007.
- [63] M. Ricchiuto and A. Bollermann. Stabilized residual distribution for shallow water simulations. *J.Comput.Phys*, 228:1071–1115, 2009.
- [64] G.L. Richard and S.L. Gavriluk. Modelling turbulence generation in solitary waves on shear shallow water flows. *Journal of Fluid Mechanics*, 773:49?74, 2015.
- [65] W. Rodi. Turbulence models and their application in hydraulics- a state of the art review. International Association for Hydraulic Research, Delf, 1980.
- [66] P. L. Roe. Approximate Riemann solvers, parameter vectors, and difference schemes. *J. Comp. Phys.*, 43:357–372, 1981.
- [67] V. Roeber. *Boussinesq-type model for nearshore wave processes in fringing reef environment*. PhD thesis, University of Hawaii, 2010.
- [68] V. Roeber, K. F. Cheung, and M. H. Kobayashi. Shock-capturing Boussinesq-type model for nearshore wave processes. *Coast. Eng.*, 57:407–423, 2010.
- [69] V. Roeber and K.F. Cheung. Boussinesq-type model for energetic breaking waves in fringing reef environment. *Coast. Eng.*, 70:1–20, 2012.
- [70] F. Shi, J. T. Kirby, J. C. Harris, J. D. Geiman, and S. T. Grilli. A high-order adaptive time-stepping tvd solver for boussinesq modeling of breaking waves and coastal inundation. *Ocean Modelling*, 43-44:36–51, 2012.
- [71] O. R. Sørensen, H. A. Schäffer, and P. A. Madsen. Surf zone dynamics simulated by a Boussinesq type model: Part III. Wave-induced horizontal nearshore circulations. *Coastal. Eng.*, 33:155–176, 1998.
- [72] I. Svendsen. Mass flux and undertow in a surf zone. *Coastal. Eng.*, 8:347–365, 1984.
- [73] C. E. Synolakis. The run up of solitary waves. *J. Fluid Mech.*, 185:532–545, 1987.

- [74] E. Tadmor. Skew-selfadjoint form for systems of conservation laws. *J. Math. Anal. Appl.*, 103:428–442, 1984.
- [75] E. Tadmor. Entropy functions for symmetric systems of conservation laws. *J. Math. Anal. Appl.*, 122:355–359, 1987.
- [76] E. Tadmor and W. Zhong. *Energy-Preserving and Stable Approximations for the Two-Dimensional Shallow Water Equations*, pages 67–94. Springer Berlin Heidelberg, Berlin, Heidelberg, 2008.
- [77] M. Tissier, P. Bonneton, F. Marche, F. Chazel, and D. Lannes. Nearshore Dynamics of Tsunami-like Undular Bores using a Fully Nonlinear Boussinesq Model. *Journal of Coastal Research*, Special Issue, 64, 2011.
- [78] M. Tissier, P. Bonneton, F. Marche, F. Chazel, and D. Lannes. A new approach to handle wave breaking in fully non-linear Boussinesq models. *Coastal Engineering*, 67:54–66, 2012.
- [79] M. Tonelli and M. Petti. Hybrid finite-volume finite-difference scheme for 2DH improved Boussinesq equations. *Coast. Eng.*, 56:609–620, 2009.
- [80] M. Tonelli and M. Petti. Finite volume scheme for the solution of 2D extended Boussinesq equations in the surf zone. *Ocean. Eng.*, 37:567–582, 2010.
- [81] M. Tonelli and M. Petti. Simulation of wave breaking over complex bathymetries by a Boussinesq model. *J. Hydraulic Res.*, 49:473–486, 2011.
- [82] M. Tonelli and M. Petti. Shock-capturing Boussinesq model for irregular wave propagation. *Coastal Engineering*, 61:8–19, 2012.
- [83] A. Viviano, R. E. Musumeci, and E. Foti. A nonlinear rotational, quasi-2dh, numerical model for spilling wave propagation. *Applied Mathematical Modelling*, 39:1099–1118, 2015.
- [84] Q. Wang, Z. Zhang, X. Zhang, and Q. Zhu. Energy-preserving finite volume element method for the improved boussinesq equation. *Journal of Computational Physics*, 270:58 – 69, 2014.
- [85] N.P. Waterson and H. Deconinck. Design principles for bounded higher-order convection schemes, a unified approach. *J.Comput.Phys.*, 224(1):182 – 207, 2007.
- [86] G. Wei and J. T. Kirby. A time-dependent numerical code for extended Boussinesq equations. *Journal of Waterway, Port, Coastal, and Ocean Engineering*, 120:251–261, 1995.
- [87] G. Wei and J. T. Kirby. A coastal processes model based on time-domain Boussinesq equations. Research report no. CACR-96-01, Center for applied and coastal research, 1996.
- [88] G. Wei, J. T. Kirby, and A. Sinha. Generation of waves in Boussinesq models using a source function approach. *Coastal Eng.*, 36:271, 1999.
- [89] G. Wei, J.T. Kirby, S. T. Grilli, and R. Subramanya. A fully nonlinear Boussinesq model for surface waves. Part 1. Highly nonlinear unsteady waves. *Journal of Fluid Mechanics*, 294:71–92, 1995.
- [90] D.C. Wilcox. *Turbulence modelling for CFD - Third edition*. DCW Inc., 2006.
- [91] N. Wintermeyer, A.R. Winters, G.J. Gassner, and D.A. Kopriva. An entropy stable nodal discontinuous galerkin method for the two dimensional shallow water equations on unstructured curvilinear meshes with discontinuous bathymetry. *Journal of Computational Physics*, 340:200 – 242, 2017.

-
- [92] J. Yan and L. Zheng. New energy-preserving finite volume element scheme for the Korteweg de Vries equation. *International Journal of Applied Mathematics*, 47(2):223–232, 2017.
- [93] Jin-Liang Yan, Qian Zhang, Zhi-Yue Zhang, and Dong Liang. A new high-order energy-preserving scheme for the modified korteweg-de vries equation. *Numerical Algorithms*, 74(3):659–674, Mar 2017.
- [94] J. A. Zelt. The run-up of nonbreaking and breaking solitary waves. *Coastal Eng.*, 15:205–246, 1991.
- [95] Y. Zhang, Kennedy A. B., A. S. Donahue, J. J. Westerink, and N. Panda. Rotational surf zone modeling for $o(\mu^4)$ Boussinesq-Green-Naghdi systems. *Ocean Modelling*, 79:43–53, 2014.



**RESEARCH CENTRE
BORDEAUX – SUD-OUEST**

200 avenue de la Vieille Tour
33405 Talence Cedex

Publisher
Inria
Domaine de Voluceau - Rocquencourt
BP 105 - 78153 Le Chesnay Cedex
inria.fr

ISSN 0249-6399